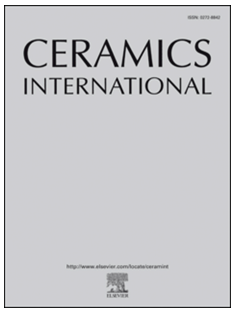

Synthesis of α-β Bi_2O_3 heterojunction photocatalyst and evaluation of reaction mechanism for degradation of RhB dye under natural sunlight

Kamal Kanti Bera, Malay Chakraborty, Mousumi Mondal, Senjuti Banik, Swapan Kumar Bhattacharya

PII: S0272-8842(19)33462-5

DOI: https://doi.org/10.1016/j.ceramint.2019.11.269

Reference: CERI 23638

To appear in: *Ceramics International*

Received Date: 2 June 2019

Revised Date: 19 November 2019

Accepted Date: 29 November 2019

Please cite this article as: K.K. Bera, M. Chakraborty, M. Mondal, S. Banik, S.K. Bhattacharya, Synthesis of α-β Bi_2O_3 heterojunction photocatalyst and evaluation of reaction mechanism for degradation of RhB dye under natural sunlight, *Ceramics International* (2020), doi: https://doi.org/10.1016/j.ceramint.2019.11.269.

To
The Editor
Ceramics International

Dear Sir/Madam,

Please find the revision of the revised manuscript CERI-D-19-05645 (ms) entitled, 'Synthesis of α-β Bi_2O_3 heterojunction photocatalyst and evaluation of reaction mechanism for degradation of RhB dye under natural sunlight' by Kamal Kanti Bera, Malay Chakraborty, Mousumi Mondal, Senjuti Banik, Swapan Kumar Bhattacharya* for your kind perusal and onward publication. The revision has been made taking consideration of all suggestions of reviewer # 2 and where we feel it necessary. The changes made are highlighted in green colour. Response to the reviewers' comments has also been attached herewith.

Hope, you will find the manuscript worthy for publication in your esteemed journal considering its importance.

Hope you will be kind enough to do the needful for publication of the paper at the earliest.

Thanking you,

Dated: 20.11.2019

Yours truly,

Swapan Kumar Bhattacharya

Department of Chemistry

Jadavpur University, Kolkata-700032, India

Synthesis of α-β Bi_2O_3 heterojunction photocatalyst and evaluation of reaction mechanism for degradation of RhB dye under natural sunlight

Kamal Kanti Bera, Malay Chakraborty, Mousumi Mondal, Senjuti Banik, ***Swapan Kumar Bhattacharya****

*Physical Chemistry Section, Department of Chemistry, Jadavpur University, Kolkata – 700032, India.

*Email – skbhatt7@yahoo.co.in

Tel. : 919831699643, Fax: +913324146584

GRAPHICAL ABSTRACT

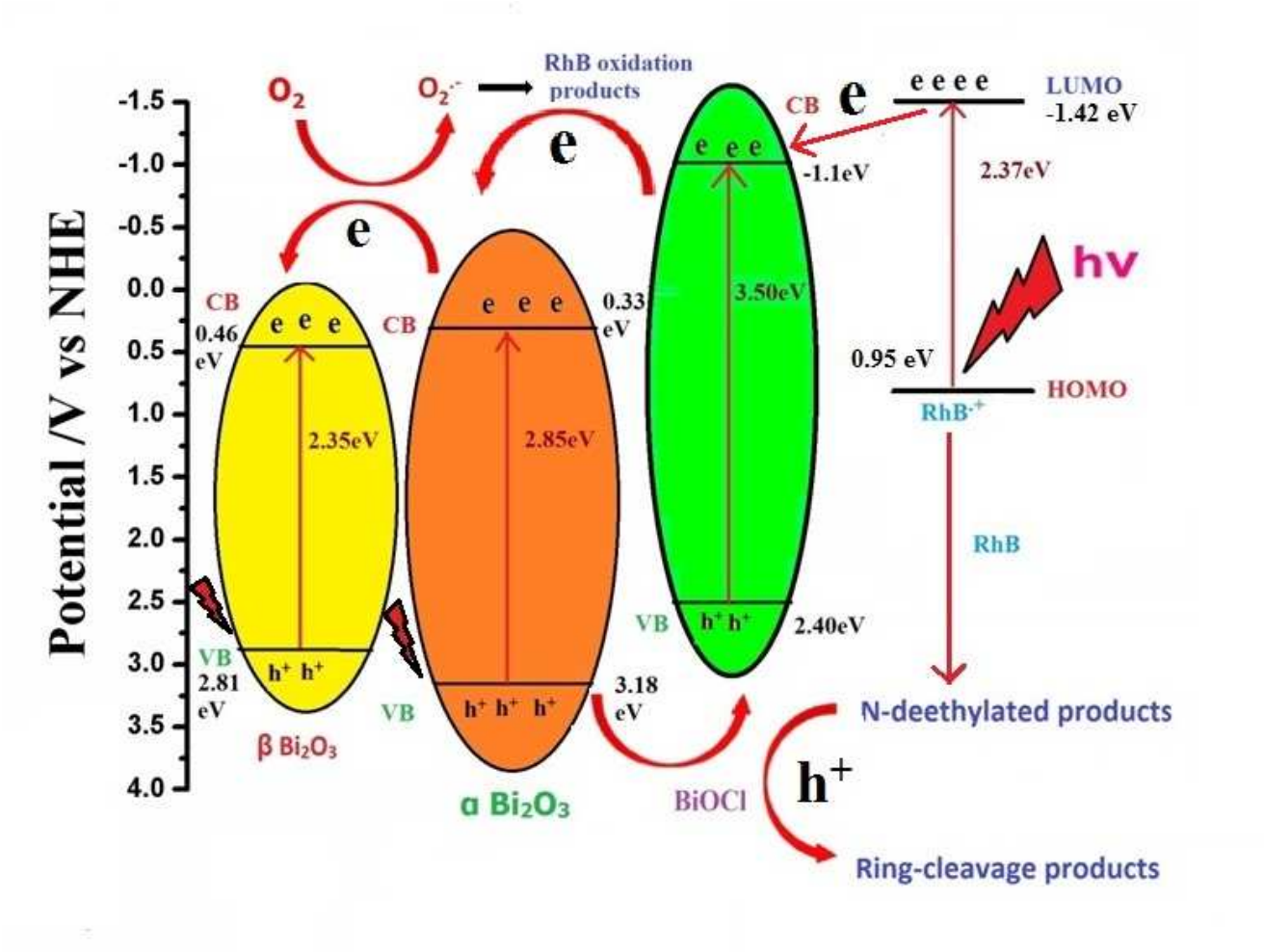

Abstract

A few biphasic nano composites containing α and β Bi_2O_3 of varying composition were synthesized by facile solvothermal method without using any capping agent and further calcination. X-ray diffraction, microscopic and spectroscopic techniques were employed for characterization of the as synthesized catalysts which are used as photocatalysts in degradation of pollutant, Rhodamine B (RhB) dye. The band gap of the nanocatalysts as calculated from tauc plot varies within 2.35- 2.58 eV for β-form and 2.85-3.19 eV for α-form in the α-β Bi_2O_3 hetrojunctions. The operational parameters that influence the degradation process were optimized. The best catalyst dosage and pH are 0.5 gL^{-1} and 4 respectively and the best concentration of H_2O_2 when added is 2 mM for 10 ppm aqueous solution of dye. Among different heterojunctions, the best catalyst which is produced from bismuth nitrate concentration of 0.05 M, degrades RhB upto 99.6% at pH 4 under 120 min sunlight irradiation. The effects of addition inorganic salts in RhB dye solution were also examined. The radical trapping experiments have been applied to explore the involved and main species responsible for degradation. The identification of degradation products of RhB was analyzed and the plausible mechanistic pathway is drawn from HPLC and HRMS. It shows that the degradation of RhB proceeds via initial generation of N-deethylated products followed by ring opening ones, which indicates the photosensitization induced photocatalytic mechanism of the reaction.

Keywords: α-β Bi_2O_3 hetrojunction; Solar remediation photo catalytic activity; Rhodamin B degradation products; Reaction mechanism

1. Introduction

In heterogeneous photocatalysis, advanced oxidation process (AOP) has been extensively used as an eco-friendly, cost-effective and green process for productive degradation of various harmful organic pollutants [1, 2] and provides solution to water quality problems. Among the various AOP, coupling of two semiconductors with different band gaps is a well-advocated strategy which increases the absorption and decreases the electron-hole recombination process. Semi-conductors like TiO_2, ZnO, Bi_2O_3, NiO [3-6] etc are usually used in AOPs. Extensive research was done on TiO_2 due to its high abundance, low cost and good stability. However high band gap (E_g 3.2eV) and poor absorption of sunlight (4-5%) [7] limit its performance. Therefore visible light active photocatalyst, Bi_2O_3 having lower band gap (2.4-2.9eV) is chosen [8] as an alternative. Among six main crystallographic polymorphs, α (monoclinic), β (tetragonal), γ (cubic bcc), δ (cubic face centred), ε (orthorhombic), ώ (triclinic), the first one is stable at low temperature, the last one at high temperature and others are metastable state [9]. A few researches on photocatalytic activity of α-β Bi_2O_3 heterojunctions are summarized in Table1 [10-17] and illustrate their importance. The table shows that the degradation efficiency of the toxic and carcinogenic dye, Rhodamin B (RhB) in natural sunlight was presented by only two previous works [12, 15]. In our previous work [12], the dependence of synthesis temperature on the composition α-β Bi_2O_3 nano heterojunction and synergistic effect on degradation of RhB over α or β Bi_2O_3 in sunlight were studied and the maximum efficiency was found to be 99.7%. In the present paper, we synthesize different α-β Bi_2O_3 heterojunctions by varying molar concentration of the precursor bismuth nitrate, studied their photocatalytic activity, optimize some degradation

Table 1: Summary of recent relevant works, synthesis and photocatalytic degradation of various dye on α-β Bi_2O_3 heterojunction catalyst.

SNo	Synthesis route	Surfactant / additive	Crystalline phase	Morphology	E_{bg}(eV)	Photocatalytic activity	Reference
1.	Solvo-thermal method	Ethylene glycol	α and β Bi_2O_3	Mixture of spheres, sheets and nanoparticles.	2.57	500W Xe lamp, 96.9% degradation of 17α-ethynylestradiol in 24 min.	Y. shi et al., 2017 [10]
2.	Solid state reaction, annealed at 650°C, 2h	-	α and β Bi_2O_3	-	2.8	9W UV light, 80% degradation of RhB in 210 min.	T. A. Gadhi et al., 2016 [11]
3.	Hydrothermal method	Glycerol	α and β Bi_2O_3	Budding flower α, spherical β	2.35(β), 2.78(α)	99.7% degradation of RhB in natural sunlight in 180 min at pH 3.	K. K. bera et al., 2018 [12]
4.	Hydrothermal	L-lysine	Selective α/β	Nanoflakes	2.85	500W xenon lamp RhB degradation rate 90% in 5h	Chen et.al, 2011 [13]
5.	Solvothermal Calcined 450^0c for 3h	Ethylene glycol	α and β Bi_2O_3	Nano spheres	2.78(α) 2.36(β)	1000W Xe lamp, Acetaminophen degradation rate93% in 180 min	Xiao et.al 2013 [14]
6.	Liquid phase microwav	Ethylene glycol	β and α Bi_2O_3	Sheet like nano particle	α(2.84), β(2.77)	91% RhB degrades in 4 hrs under sunlight	Qiu et. al, 2011

	e reaction, calcined 300^0c for 5 hrs						[15]
7.	Hydrothermal Calcined 300^0c for 5 hrs	Benzyl alchol	α and β Bi_2O_3	Sheets, nanowires, nanocrystal	2.71(α/β) 2.48(β)	300W Xe lamp, Rhodamine B degradation rate 98% (α/βcomposite) and 85% (β Bi_2O_3) in 60 min.	Hou et. al, 2013 [16]
8.	Electrospinning	Poly(ethylene-co-butylene)-block-poly(ethelene oxide) di block copolymer, calcined 400^0c	Mixture of α and β Bi_2O_3	Electrospun fiber mats	3.4	8W UV lamp,76% RhB , excellent photocatalytic activity.	Brezesinski et.al 2010 [17]

parameters like pH, effective catalyst dosage in details and the effect of addition of H_2O_2 and inorganic salt like Cl^-, NO_3^-, SO_4^-, CH_3COO^- in sunlight. The degradation intermediates of RhB by α-β Bi_2O_3 photocatalyst in natural sunlight were also identified with assistance of high resolution mass spectroscopy (HR-MS) and high performance liquid chromatography (HPLC) study.

2. Methods

2.1 Synthesis of Bi_2O_3 nano crystal

All chemicals were analytical reagent grade and used without purification. In this experiment, α-

β Bi_2O_3 heterojunctions were synthesized by a facile hydrothermal method. In a typical synthesis, 0.02 (M) Bismuth nitrate pentahydrate [$Bi(NO_3)_3$, $5H_2O$] was dissolved at first in 50 mL glycerol with sonication for 1 h followed by constant stirring for 3 h. Then it was transferred into a 100 mL teflon-lined stainless steel autoclave, sealed and heated at 180^oC for 4 h. The system was then cooled at room temperature and the product obtained by filtration, washed several times with distilled water and ethanol and finally dried in vacuum desiccators at room temperature. Other catalysts were prepared by changing the precursor concentration from 0.02 (M) to 0.3 (M) keeping other procedure same. The precursor concentrations are taken 0.02 (M), 0.03 (M), 0.05 (M) and 0.3 (M) and the corresponding products are coded as S1, S2, S3 and S4. The reaction of glycerol with bismuth nitrate is shown in the Scheme 1[14].

Scheme 1

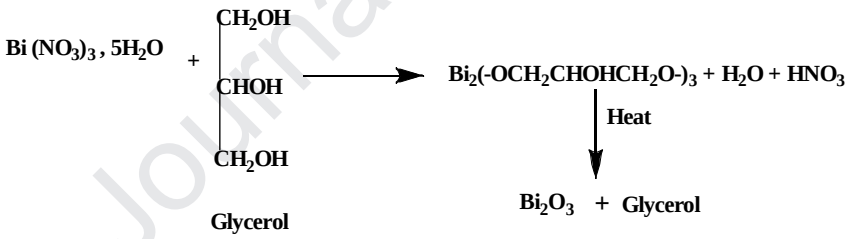

Scheme 1. Synthesis of Bi_2O_3.

2.2 Structural characterization

X ray powder diffraction (XRD) study was carried out using a difractomter (Bruker D8 Advance) equipped with a CuKα radiation source (λ= 1.5418A^o generated at 40 KV and 40 mA). The morphologies of obtained materials were inspected by a field emission scanning electron microscopy (FESEM, INSPECT F50 FEI), transmission electron microscopy (TEM), high-resolution transmission electron microscopy (JEM-2100 HRTEM, JEOL, Japan, operated at

200Kv), selected-area electron diffraction (SAED) and energy dispersion X ray spectroscopy (EDX). The ex- situ Fourier transform infra-red spectroscopy (FTIR) of synthesized materials were carried out using spectrophotometer (Perkin Elmer, SN-74514, spectrum RX1 and resolution 4 cm^{-1}). Absorption spectra were recorded using a model V-630 UV-visible spectrophotometer (Jasco, Japan) within the wavelength range of 400-600 nm. Nitrogen adsorption and desorption experiment was carried at 77 K in a NOVA 2200e, Quantachrome Instruments, USA, specific surface area and pore size analyzer. In this measurement, the samples were first degassed under vacuum condition for 8 h at 423 K. The surface charge of Bi_2O_3 was characterized by Zeta potential analyzer (Zetasizer nano ZS (Malvern,UK) at 90° scattering angle with a He-Ne Laser(λ= 632.8nm)

2.3 Photocatalytic experiments

The photocatalytic activities of the synthesized Bi_2O_3 nano particles were carried out by photo degradation of Rhodamine-B under sunlight. 100 mL of 10 ppm of aqueous suspension of Rhodamine B containing 0.5 gL^{-1} of Bi_2O_3 nano particles agitated by a magnetic stirrer (500 rpm) in the dark to make the dye- adsorbed catalyst in the well dispersed state in the solution. Then it was exposed to sunlight and 4 mL solution was withdrawn at every 15 min interval, centrifuged and filtered. The residual dye solution was analyzed spectrophotometerically and the changes in the concentration of Rhodamine-B were observed from its characteristics absorption at the wavelength of absorption maximum, 554 nm. To keep the consistency in irradiation of natural sunlight all the photocatalytic experiments were intentionally performed between 11.00 a.m. to 2.30 p.m. in consecutive sunny days during February and March, 2018 (Jadavpur, Kolkata, India). Besides a digital lux meter (LX 101A.) is used to measure time dependent light

intensity of natural sunlight from which average illumination is obtained. The photo catalytic degradation was calculated as follows:

$$\% \text{ Photocatalytic degradation} = \{(C_0-C_t)/C_0\} \text{x } 100$$

Where C_0 is the initial absorbance and C_t the absorbance of the sample after irradiation for time t minute.

2.4. Trapping Experiment

The method of trapping experiment is the same to the photocatalytic degradation experiments; only difference is the addition of different scavengers. In this experiment we used 2 mM of different scavengers like Parabenzoquinone (BQ), Isopropyl alcohol (IPA) and Sodium-EDTA (Na_2EDTA) as $\cdot O_2^-$, $\cdot OH$ and h^+ trappers respectively.

3. Result and discussions

3.1 Characteristics of Bi_2O_3 nano particles

Fig. 1 illustrates the XRD patterns of as-prepared samples. The sample S1, S2, S3 exhibits peaks having 2θ (/degree) values at 28.00, 30.18, 32.90, 42.16, 53.40, 62.93, 68.56, 78.35 corresponding to (201), (211), (220),(320), (322), (422), (432), (314) planes of tetragonal β-Bi_2O_3 respectively [JCPDS NO 78-1793] and the peaks having 2θ(/degree) at 23.92, 29.36, 35.09, 47.33, 54.67, 56.56 can be attributed to ($1\bar{1}1$), (311), (210), (420), (014), (240) planes of monoclinic α-Bi_2O_3 respectively [JCPDS NO 72-0398]. XRD pattern recorded for sample S4 contains peaks at 2θ (/degree) values of 30.18, 32.90, 39.72, 42.16, 53.22, 62.23, 64.63 corresponding to the (211), (220), (320), (402), (322), (422), (520) planes of tetragonal β-Bi_2O_3 [JCPDS NO 78-1793] and peaks at 2θ values of 23.92, 27.12, 37.83, 44.71, 46.13, 48.71, 56.12,

70.72 for ($1\bar{1}1$), (112), ($1\bar{1}2$), (510), (040), (041), (104), , (061) planes of monoclinic α-Bi_2O_3 [JCPDS NO 72-0398] respectively. The size of crystallites of the samples was measured using the Debye-Sherrers equation [18]. From XRD data we concluded that our synthesized samples were the mixtures of α and β phases of Bi_2O_3 with various compositions and with crystallite size in the range of 6-42 nm. The composition of heterojunction with different β/α phase is also a function of molar concentration of the precursor. Table 3 presents the relative ratio of intensity of one dominant peak of β at 2θ = 32.90° (corresponding to 220 plane) to another significant peak intensity of α at 2θ = 27.10° (corresponding to 112 plane) for different synthesized samples. The data reveal that the relative increase of β over α phase continues up to concentration limit of 50 mM of the precursor. At higher concentration of $Bi(NO_3)_3$ like 300 mM, the heat rejection is relatively slow during cooling of autoclave and thus the α form which is more stable at higher temperature predominates. Notably, pure α and β form can be obtained by the calcination of α-β Bi_2O_3 at 400°C and 250°C respectively in hydrothermal method [12]. Thus the relative composition of α and β in α-β Bi_2O_3 heterojunctions can be monitored by changing the concentration of the precursor in the hydrothermal synthesis.

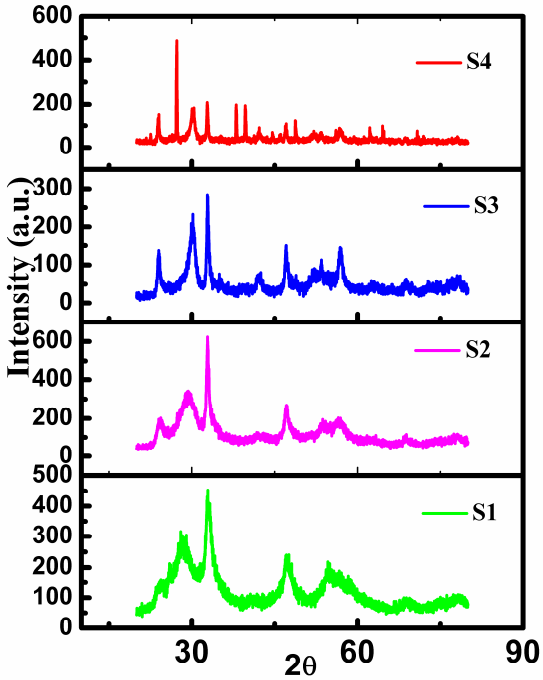

Fig. 1. The XRD patterns of four (S1-S4) α-β Bi_2O_3 heterojunctions synthesized at different concentration of precursor.

Fig. 2 a, b and c. demonstrate the FESEM images of S1, S3 and S4 α-β Bi_2O_3 composites respectively. From Fig. 2 it is seen that the S1 catalyst contains the mixture of nano sphere of diameter 24 nm and nano rod like structures with average 126 nm lengths and 40 nm breadths. S3 catalyst displays nano flake like structures which are made by spherical particles of average diameter 28 nm. S4 catalyst shows the budding flower like morphology. The representative EDS spectrum of some parts of S1 (Fig. 2d) confirms the formation of Bi_2O_3 in the photo catalysts as Bi and O atom are present in the ratio of 2: 3.06.

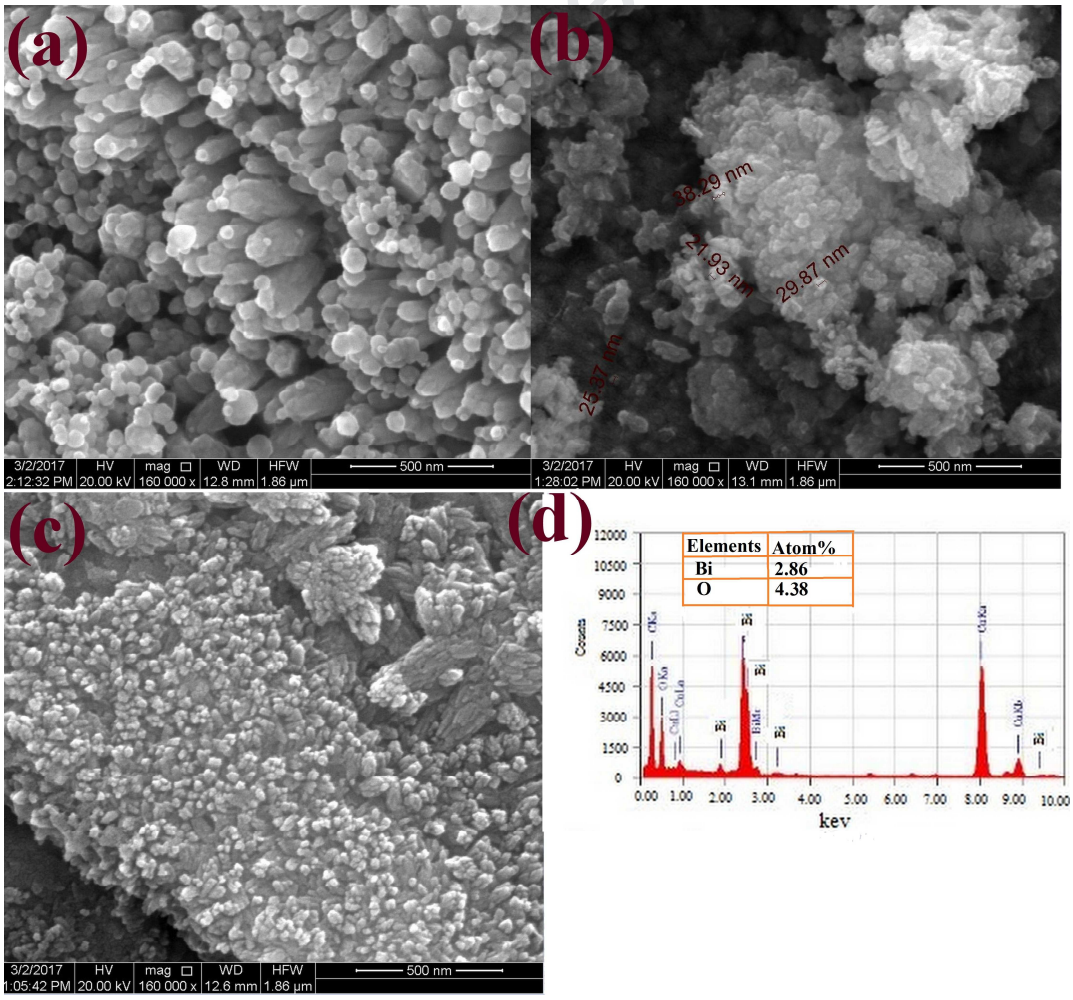

Fig. 2. The FESEM images of (a) S1 (b) S3 (c) S4 photocatalyst (d) EDX image of representative α-β Bi_2O_3 heterojunction.

The TEM images of S3 catalyst (Fig. 3a and b) indicate that the catalyst is composed of porous nano flakes of Bi_2O_3. The average size of the pores as determined by bar diagram is about 4.04 nm. The HRTEM image presented in figure 3c displays the lattice spacing of 0.31 nm and 0.37 nm corresponding to the inter planner spacing of (201) of β and $(\bar{1}11)$ of α Bi_2O_3 which further confirm a phase junction between α Bi_2O_3 and β Bi_2O_3. Selected-area electron diffraction (SAED) profile (Fig. 3d) exhibits also α and β planes matched with the XRD results.

N_2 adsorption- desorption isotherm measurements were carried out to evaluate the specific surface areas, pore volumes and the average pore size distributions of the as prepared samples. The BET surface area (m^2g^{-1}) of S1-4 samples was found to be 19.6, 11.5, 49.1 and 4.24 and Barrett-Joyner-Halenda (BJH) desorption analyses for the composites exhibit that the least value of average pore-diameter (2.68 nm) is obtained with S3 among all the synthesized materials. The highest surface area (11.5 times than S4 catalyst), the largest total pore volume (0.108 cm^3g^{-1}) and the smallest pore diameter (2.68 nm) of S3 catalyst (Table 2) could supply more surface active sites and make transport easier leading to an enhancement of photocatalytic performance. According to the Brunauer-Deming-Deming-Teller (BDDT) classification, the isotherms (Fig.4a) can be categorized as Type IV hysteresis loop indicating the formation of mesoporous materials [16, 19-20]. Fig.4b provides the Pore size distributions of as-synthesized α-β Bi_2O_3 heterojunctions (S1-S4).

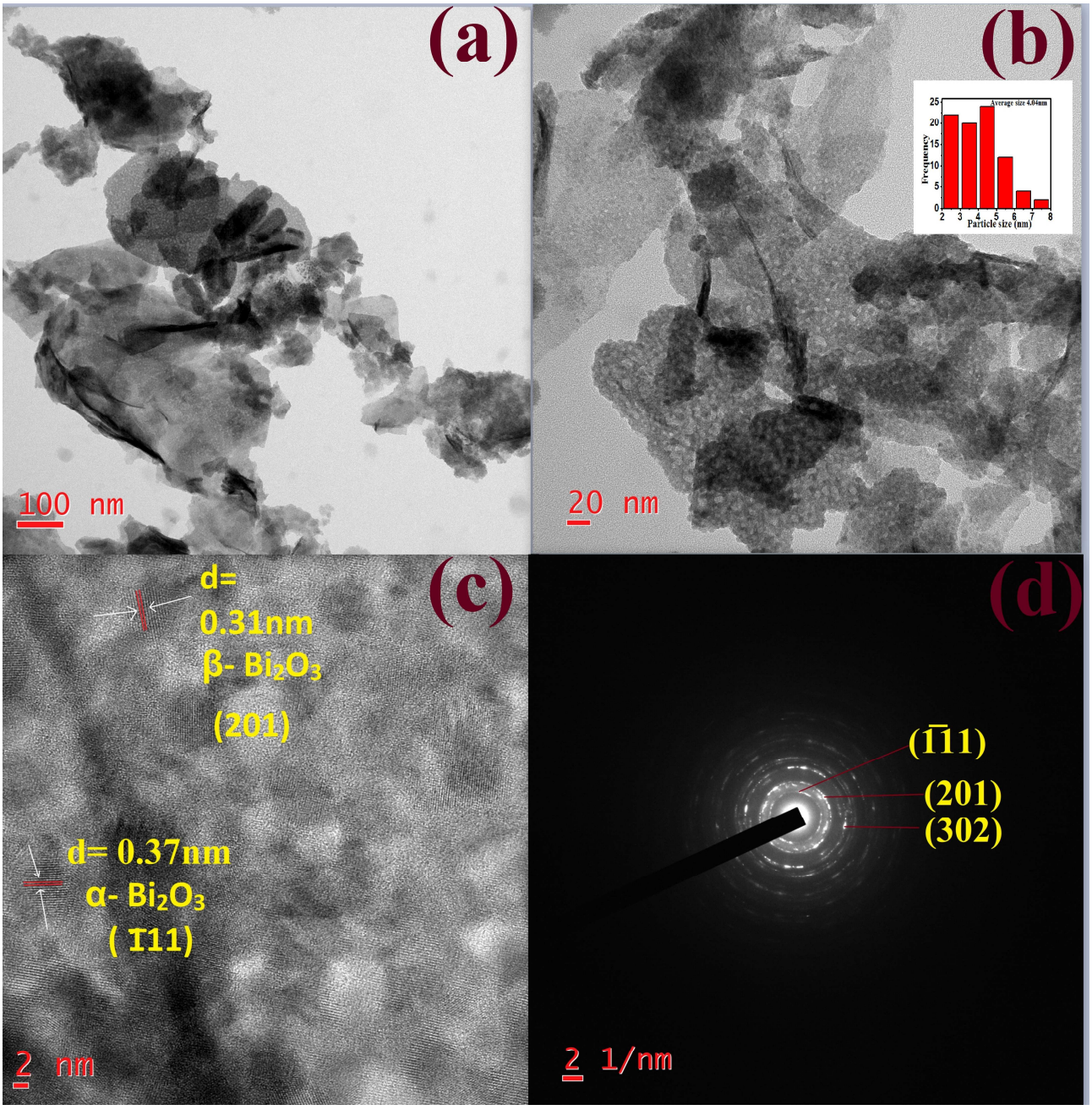

Fig. 3. (a) The TEM image at a given magnification and (b) same image at higher magnification (c) HRTEM image (d) SAED pattern of S3 catalyst.

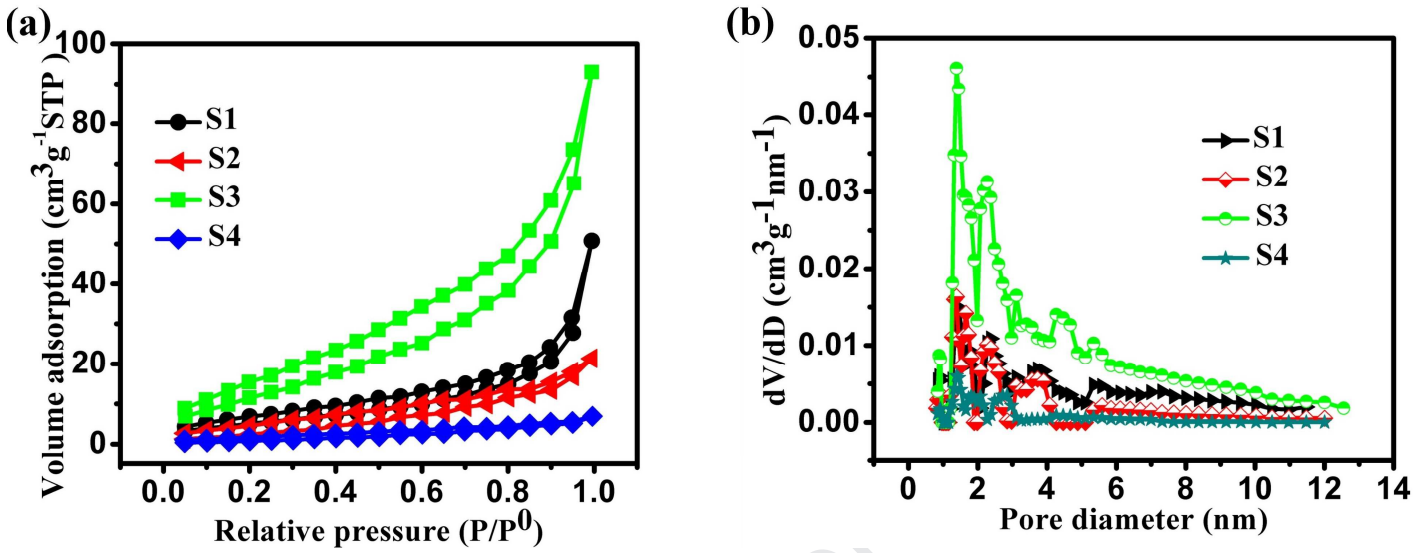

Fig. 4. (a) N_2 adsorption-desorption isotherms (b) Pore size distributions of as-synthesized α-β Bi_2O_3 heterojunctions (S1-S4).

Table 2. BET surface areas, total pore volume and mean pore size of synthesized catalysts.

Semiconductor	Surface area (S_{BET}), m^2g^{-1}	Total pore volume (V_{Total}), cm^3g^{-1}	Average pore diameter (nm)
S1	19.6	0.046	2.78
S2	11.5	0.026	2.76
S3	49.1	0.108	2.68
S4	4.24	0.008	2.88

Fig. 5 illustrates the FTIR spectra of different α-β Bi_2O_3 heterojunctions (S1-4). The band at 850 cm^{-1} is attributed to the symmetrical stretching vibration Bi-O bond of the BiO_3 species [12, 21] and the band 768 cm^{-1} originates from the metal oxygen vibration [22]. The band at 1558 cm^{-1} is related to the vibration of the residual hydroxyl group (Bi_2O_3–OH) [23] and the weak broad band centered around 3322 cm^{-1} is possibly due to the stretching vibration of O-H bond of very small number of adsorbed H_2O molecules [24, 25]. The band at 1386, 1287 and 1459 cm^{-1}can be related to the C-O stretching vibrations and –C-H bending vibration of the adsorbed ethanol [26, 27]. The band at 921 cm^{-1} is the characteristic stretching vibration of Bi-O bond in strongly distorted BiO_6 octahedral units [28].

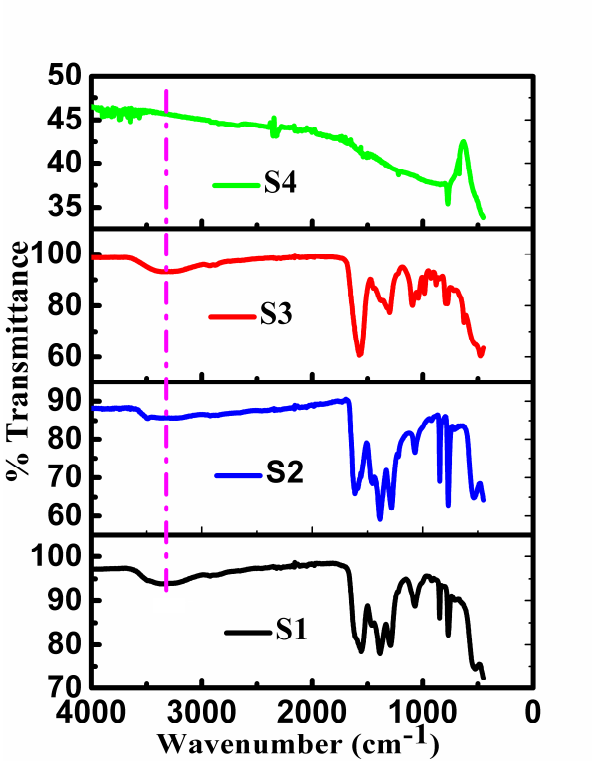

Fig. 5. FTIR spectra of synthesized α/β Bi_2O_3 nano hetero-junctions (S1- S4).

The optical properties of synthesized α-β Bi_2O_3 are followed by UV-vis absorption spectroscopy.

The order of absorbance of the heterojunctions is S3 > S1 > S2 > S4 where corresponding profiles are exhibited in the Fig. 6a. Table 3 reveals that S1- S2- S4 size increases, surface area decreases and absorbance decreases. Greater absorbance of S3 is due to high β content. In earlier report we find that the absorbance of β Bi_2O_3 is enhanced in the visible light region compared to α Bi_2O_3 [29]. The band gap energy (E_g) was evaluated using Tauc plot as done in our previous work [12]. The plot of $(\alpha h\nu)^2$ vs hν for each composite exhibits two different slopes of the tangents from which the bands of α and β phases of Bi_2O_3 are obtained as depicted in Fig. 6b and Table 3 respectively. The band gap varies 2.35-2.58 and 2.85- 3.19 for β and α phases in α-β Bi_2O_3 heterojunctions respectively. The obtained band gap values are consistent with the previous results [12, 16, 25- 31].

(a) **(b)**

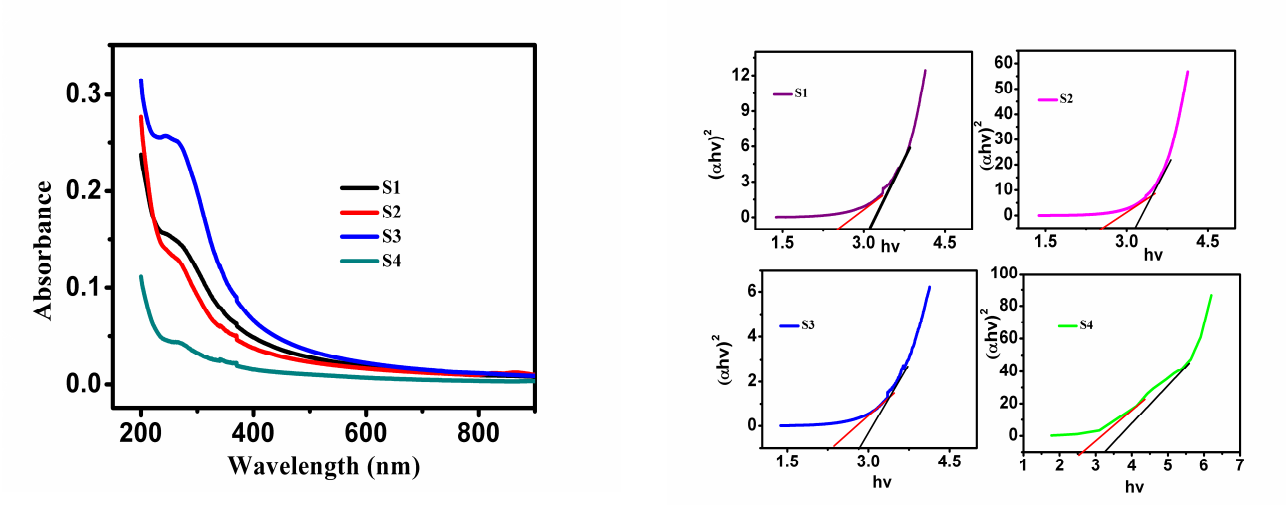

Fig. 6. (a) UV-vis spectra of S1-S4 photo-catalysts. (b) $(\alpha h\nu)^2$ vs hν profiles of S1-S4 photo-catalysts for the determination of band gap energy.

3.2. Influence of reactant concentration

The size of synthesized Bi_2O_3 nano particles has also great dependence on the concentration of $Bi(NO_3)_3$ solution in the hydrothermal synthesis. Fig. 7 represents the variation of particle size with concentration of reactant. From the Fig. 7 it is seen that average particle size gradually increases from 6 nm to 42 nm when concentration of reactant changes from .02 (M) to 0.3 (M). In general, when concentration the reactant was low, the synthesized particles are accumulated in different localized zone and agglomerate as glycerol is highly viscous [32]. As the ratio bismuth nitrate: glycerol increased, accumulation of particles was greater causing agglomeration and higher particle size.

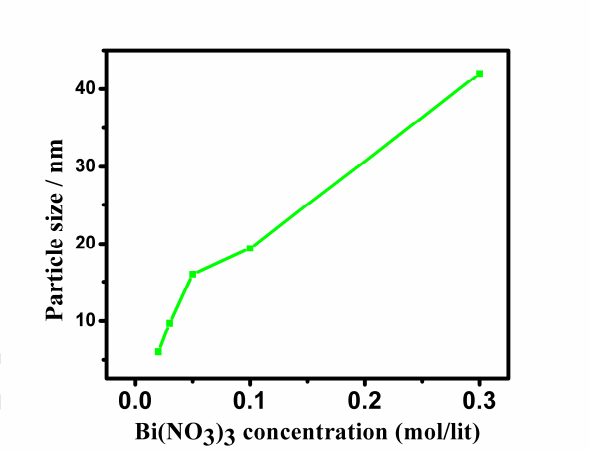

Fig. 7. Effect of precursor concentration on the average size of the synthesized particles which are obtained by heating hydrothermally at temperature 180°C for 6 h, all other parameters being unchanged.

4. Photocatalytic experiment of Rhodamine-B

4.1 Effect of irradiation time

To evaluate the photocatalytic activity of synthesized α-β Bi_2O_3 photocatalysts, the degradation of RhB are performed upto 180 min under sunlight. The degradation profiles of S1, S3 and S4

catalysts are exhibited in Fig. 8 a, b and c respectively. The plot of c/c_0 versus time in Fig. 8d exhibits 84.4, 80.2, 89 and 31.2 % degradation of RhB and associated rate constant of the reaction in min^{-1}, are 0.194, 0.133, 0.02037 and 0.00201 for S1, S2, S3 and S4 catalysts respectively.

Table 3. Synthetic, physiochemical and kinetic parameters of various α-β Bi_2O_3 heterojunctions.

Catalyst	$Bi(NO_3)_3$concentration taken (mM), reaction temperature and time of reactions are 180°C and 4 h respectively in each case.	Relative peak intensity ratio of β at (2θ =) 32.90°and α phase having 2θ at 27.10°	Average crystallite size (nm)	Band gap (eV)	% degradation of RhB in 120 min	Rate constant (k/min^{-1})
S1	20	1.89	6	2.53 (β), 3.15 (α)	84.42	0.01944
S2	30	2.18	9.7	2.48 (β), 3.12 (α)	80.24	0.0133
S3	50	3.72	20	2.35 (β), 2.85 (α)	89.01	0.0208
S4	300	0.46	42	2.58 (β), 3.2 (α)	31.27	0.00201

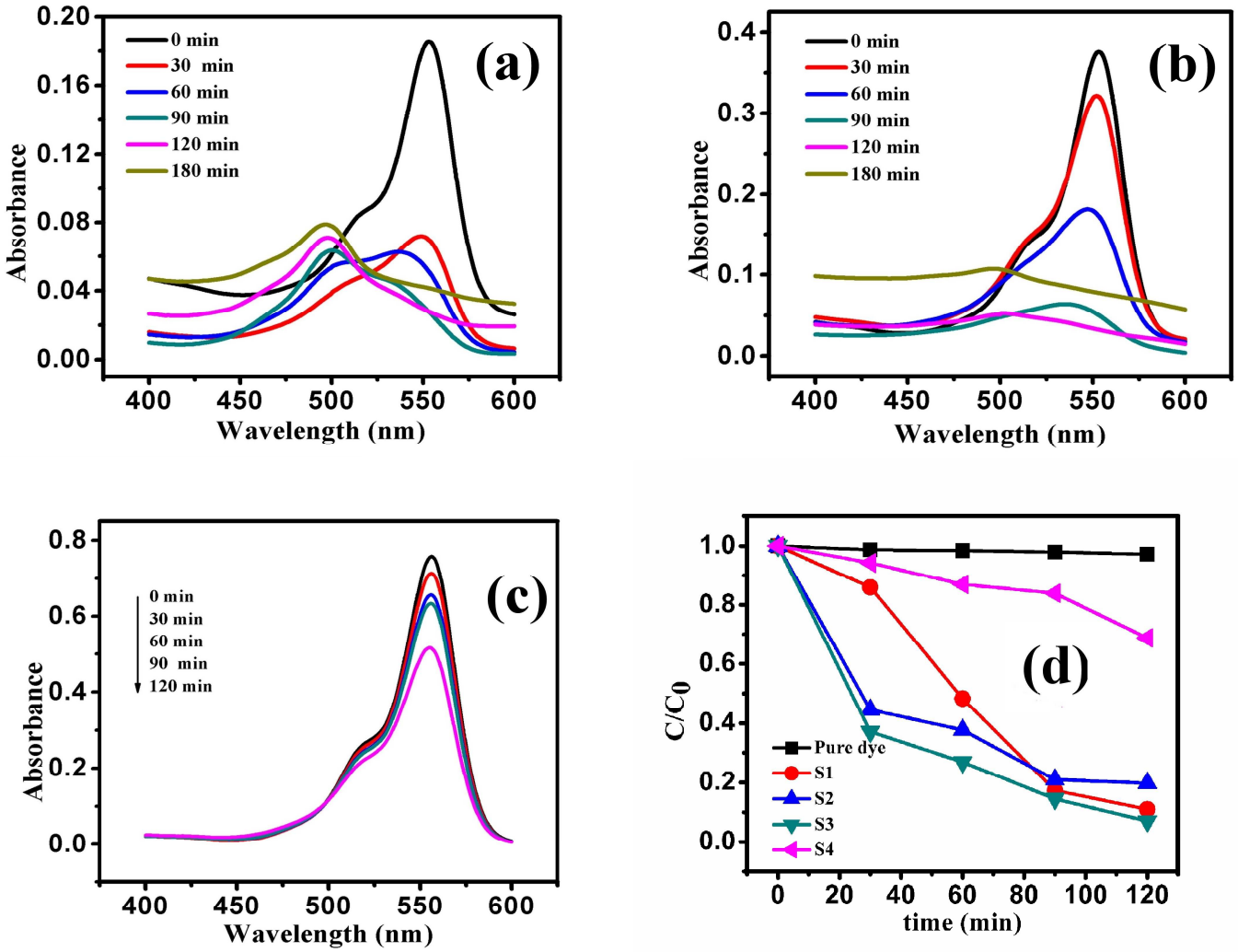

Fig. 8. UV-vis spectra of RhB degradation at different time intervals using (a) S1 (b) S3 (c) S4 catalyst and (d) Plot C/Co versus time for pure dye and S1-S4 catalysts [RhB] $=1\times10^{-5}$ M, [catalyst] = 0.5 g/L. and AI = 490×100 lux.

The degradation rate is the highest for S3 catalyst and 10 times greater than S4 catalyst. This is due to the high β/α ratio, lower size and lower band gap in S3 catalyst compared to S4. The degradation rate also slightly decreased for S2 compared to S1 catalyst because of greater size of the later. From Fig. 8a and b, it is shown that the spectral maximum shifted to 554 to 496 nm gradually after 60 min irradiation in sunlight and the color of the solution changed from red to colorless. The decrease in absorbance and hypsochromic shift in absorption spectra is due to

breaking down of RhB structure and step by step de-ethylation respectively [33, 34]. The influence of degradation parameters like catalyst dosage, pH, addition of H_2O_2 and inorganic salt in presence of α-β Bi_2O_3 (S3) catalyst are discussed below.

4.2 Effect of solution pH

The degradation was studied in the pH range 2-12 (Fig. 9a) and adjusted by addition of strong HCl and NaOH solutions. The figure shows that S3 catalyst (0.2 gL^{-1}) degrades RhB dye (10 ppm) upto 94% in 60 minute at pH 4. The rate constant ($x10^2$) values (min^{-1}) are 3.26, 6.28, 5.14, 2.84, 1.71 and 1.67 at pH 2, 4, 6, 8, 10 and 12 respectively. It reveals that the degradation is very poor at both very low and high pH. At very low pH, increased concentration of Cl^- might act as a scavenger of h^+ and $^{\cdot}OH$ radical [10]. At very high pH, the holes may be absorbed by OH^- ions producing $^{\cdot}OH$ radical which otherwise engages to produce H_2O_2 and decomposition of dye [12]. The rate constant values exhibit a maximum at pH 4 as evident from the lower inset of figure 9a. The surface charge of the Bi_2O_3 nano particles was determined by Zeta potential measurement. For its measurement Bi_2O_3 suspensions (0.1 gL^{-1}) were prepared and the pH was adjusted between 1-10 using 1 mol Lit^{-1} NaOH or HCl solutions [35]. The Zeta potential (ζ) of Bi_2O_3 catalyst at different pH conditions was measured to determine the effect of pH values on the surface charge of Bi_2O_3. The change of ζ of S3 catalyst (Fig. 9b) shows an evident decrease with increasing pH values. At pH 2, value of ζ is 8.17 mV and pH 3 it becomes -9.41mV. The point of zero charge (PZC) of the Bi_2O_3 is estimated to be 2.45. At pH (4) > PZC (2.45), surface of Bi_2O_3 becomes negatively charged. Therefore, -vely charged Bi_2O_3 particles facilates the adsorption of + vely charged diethylamine group in RhB molecules owing to electrostatic attraction and more adsorption of RhB dye on the COO^- part of zwitter ionic RhB dye (since its pKa is 3.1). This also infers that degradation of RhB undergoes via N-deethylation mechanism predominantly [36].

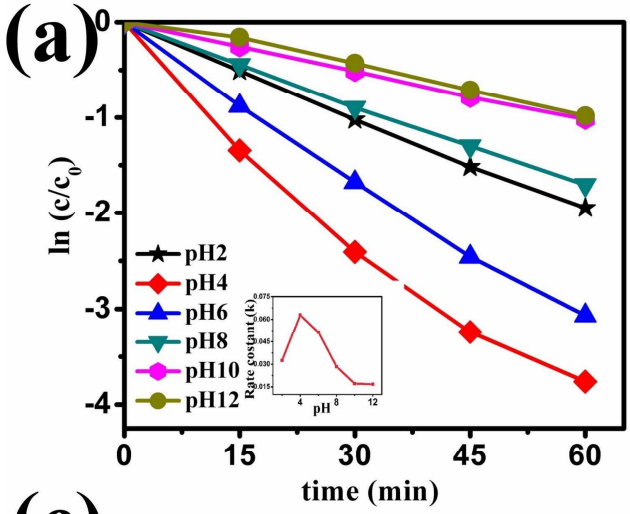
(a)
ln (c/c0)
time (min)
pH2
pH4
pH6
pH8
pH10
pH12
Rate gostant (k)
pH

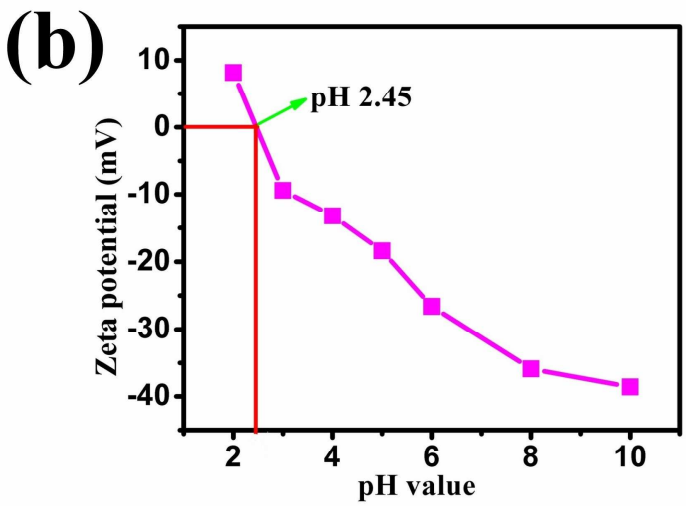
(b)
Zeta potential (mV)
pH value
pH 2.45

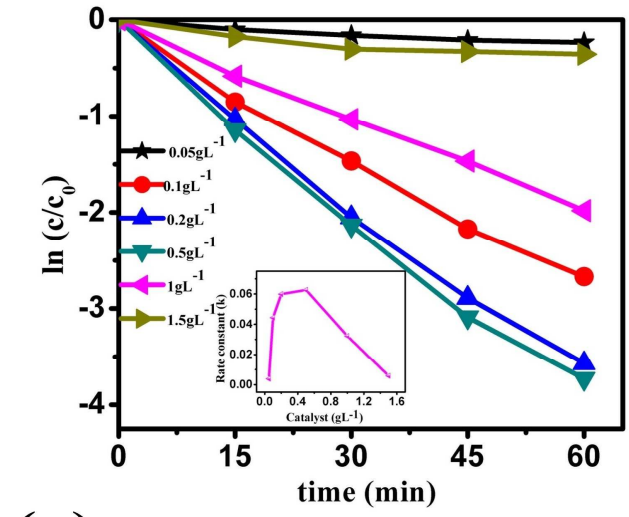
(c)
ln (c/c0)
time (min)
0.05gL-1
0.1gL-1
0.2gL-1
0.5gL-1
1gL-1
1.5gL-1
Rate constant (k)
Catalyst (gL-1)

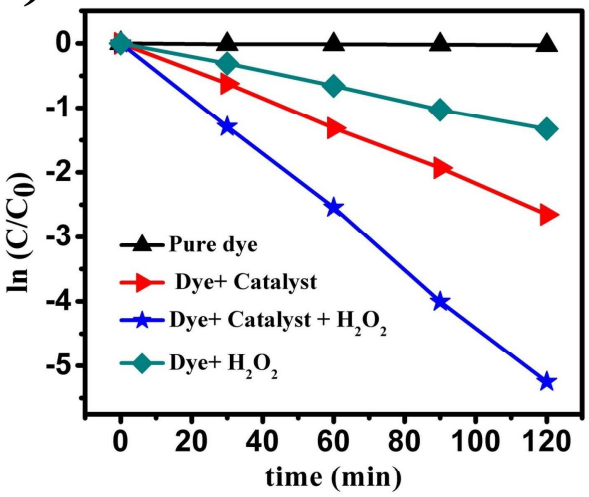
(d)
ln (C/C0)
time (min)
Pure dye
Dye+ Catalyst
Dye+ Catalyst + H2O2
Dye+ H2O2

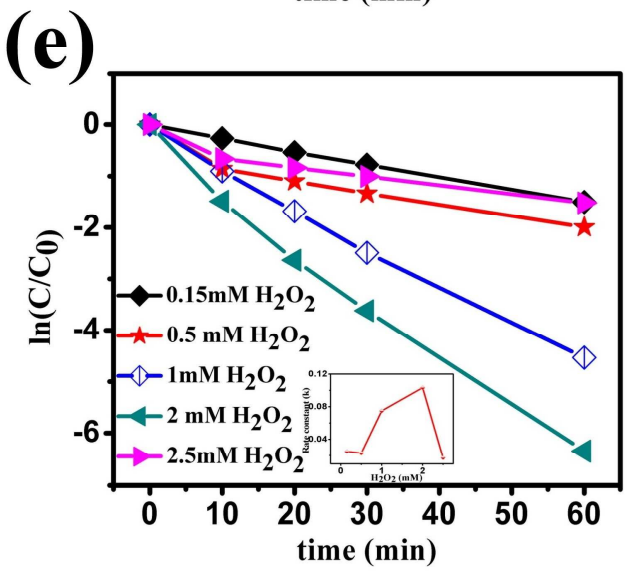
(e)
ln(C/C0)
time (min)
0.15mM H2O2
0.5 mM H2O2
1mM H2O2
2 mM H2O2
2.5mM H2O2
Rate constant (k)
H2O2 (mM)

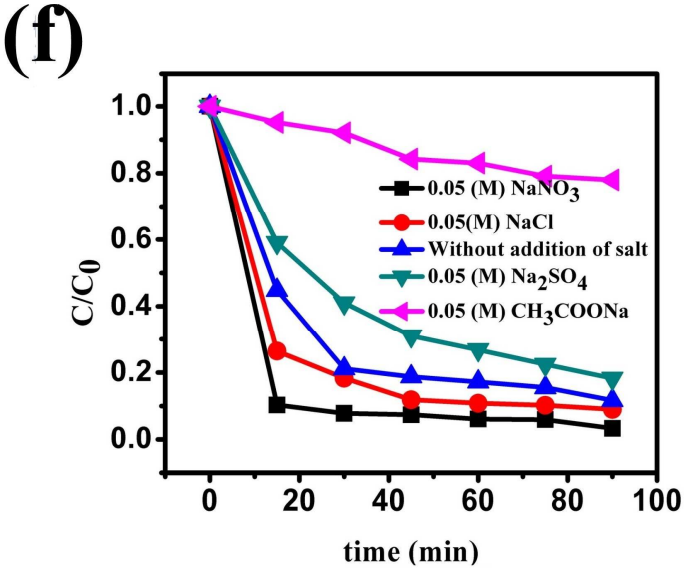
(f)
C/C0
time (min)
0.05 (M) NaNO3
0.05(M) NaCl
Without addition of salt
0.05 (M) Na2SO4
0.05 (M) CH3COONa

Fig. 9 (a) effect of solution pH on chronodegradation of RhB. Initial concentration and catalyst are $1x10^{-5}$ M and $0.2gL^{-1}$. (b) Effect of pH on the zeta potential of S3 composite in aqueous solution (T = 25° C). (c) Effect of dosages of S3 catalyst on chronodegradation of RhB upto 60 min, initial concentration of which is 10^{-5} M at pH 4. The variation of rate constant with pH and catalyst dosages is presented at the lower inset of each figure. The average illumination (AI) of the natural sunlight during the experiment was 630 x100 lux. (d) Degradation profile of RhB in presence or absence of H_2O_2 [dye] =$1x10^{-5}$ M, [catalyst] = 0.5 gL^{-1}, pH=4, AI= 480x100 lux., irradiation time 120 minutes under sunlight. (e) Effect of variation of H_2O_2 concentration on degradation .The lower inset represents apparent rate constant of degradation versus H_2O_2 concentration in the solution. (f) Plot C/Co versus time for the addition of inorganic salt in the photo catalytic degradation of RhB.

4.3 Effect of catalyst dosage

The optimum value of catalyst dosage obtained by studying with various concentration of S3 catalyst from 0.05 gL^{-1} to 1.5 gL^{-1} taking 10 ppm RhB solution at pH 4 (Fig. 9c). The degradation is achieved by 98% with 0.5 gL^{-1} in 60 min. The rate constant (x100) values (min^{-1}) are 0.387, 4.44, 5.99, 6.27, 3.23 and 0.578 for 0.05, 0.1, 0.2, 0.5, 1, and 1.5 gL^{-1} respectively. The variation of rate constant with catalyst dosage is presented at the lower inset of figure 9c. It exhibits initial increase of degradation efficiency plausibly because of increasing number of reaction sites on the catalyst surface. Again it decreases with higher loading is due to the light scattering effects and self quenching of excited catalyst molecules [37-40].

4.4 The effect of addition of H_2O_2

The effect of addition of H_2O_2 on the degradation of RhB (Fig. 9d) in presence of catalyst under natural sunlight was also studied. When 1 mL of 2 mM H_2O_2 (30%) is added to 100 mL of 10 ppm dye solution, it degrades 99.6% and 89% in presence and absence of H_2O_2 respectively in 120 min. H_2O_2 increases the rate of degradation of RhB by 10.6% . The rate constant values are $2.1x10^{-4}$, $1.1x10^{-3}$, $2x10^{-2}$, and $4.4x10^{-2}$ min^{-1} for pure dye, dye with H_2O_2, dye with catalyst and dye with both catalyst and H_2O_2 respectively. The rate constant value of the dye in presence of catalyst increases 2.16 times on addition of H_2O_2 to it.

In order to investigate the effect of H_2O_2 concentration on the degradation kinetics, different quantity of H_2O_2 is added to the solution keeping other parameters constant. Fig. 9e reveals that the rate constant of the decolonization reaction increases by 32.7% in 60 min with increasing concentration of H_2O_2 from 0.15 mM to 2 mM. This might be due to increase of $^{\bullet}OH$ radical concentration on increasing the concentration of H_2O_2 in the solution.

The increase of H_2O_2 concentration further results in decrease of removal of color by 20.4%. Therefore the concentration of H_2O_2 kept at an optimum level (2 mM). This might be due to the fact that at high concentration very reactive $^{\bullet}OH$ radical could be consumed by H_2O_2 and results in the generation of less reactive $^{\bullet}OOH$ radical which has lower oxidation capabilities than $^{\bullet}OH$ [41] and as be illustrated by the following Eqs.(1)- (3).

$$H_2O_2 + hv \longrightarrow {}^{\bullet}OH \quad (1)$$

$$H_2O_2 + {}^{\bullet}OH \longrightarrow HO_2^{\bullet} + H_2O \quad (2)$$

$$HO_2^{\bullet} + {}^{\bullet}OH \longrightarrow H_2O + O_2 \quad (3)$$

4.5 Effect of inorganic salts

The photo-catalytic degradation may be affected by many organic and inorganic species present in the real industrial waste water. In this study, the effect of NO_3^-, Cl^-, SO_4^{2-}, CH_3COO^- ions on RhB dye was investigated and depicted in Fig. 9f. From the figure, it is seen that the % of degradation of RhB in presence of NO_3^-, Cl^-, SO_4^{2-}, CH_3COO^- ions are 96.7, 93.6, 81 and 22% respectively. Notably, % of degradation in absence of any such ions is 88% in 90 min. The higher degradation efficiency in presence of NO_3^- ion is due to strong adsorption of nitrate ions on α-β Bi_2O_3 surface and production of ·OH radicals from photo induced aqueous nitrate in sunlight [42-44] as shown in the Eq. (4) - (7).

$$NO_3^- + hv \longrightarrow \cdot NO_2 + \cdot O^- \quad (4)$$

$$\cdot O^- + H_2O \longrightarrow \cdot OH + OH^- \quad (5)$$

$$NO_3^- + hv \longrightarrow NO_2^- + O(^3P) \quad (6)$$

$$NO_2^- + O(^3P) + hv \longrightarrow NO + \cdot OH \quad (7)$$

It has been illustrated in our previous result [12] that the introduction of Cl^- into the reaction mixture of degradation causes modification of Bi_2O_3 surface by producing BiOCl which can also assist the degradation process [11] but Cl^- ion also acts as ·OH radical scavenger by the following Eq. (8) - (11) [45, 46]. So, the rate in presence of Cl^- decreases little bit compared to that in presence of NO_3^-.

$$Cl^- + h^+ \longrightarrow Cl\cdot \quad (8)$$

$$Cl^- + \cdot OH \longrightarrow ClOH\cdot^- \quad (9)$$

$$2\,Cl^- \longrightarrow Cl_2 + 2e \quad (10)$$

$$Cl_2 + H_2O \longrightarrow HOCl + Cl^- + H^+ \quad (11)$$

For SO_4^{2-} ions, they are adsorbed in the surface of the Bi_2O_3 and reacts with photo induced holes (h^+) to form SO_4^- [47, 48]. This generated sulfate radical also helps the degradation process

according to the following Eqs. (12) and (13) but it also acts as a holes scavenger. So, degradation rate decreases compared to nitrate and chloride ion.

$$h^+ + SO_4^{2-} \longrightarrow SO_4^{\cdot-} \quad (12)$$

$$SO_4^{\cdot-} + e^- (\text{or } H_2O) \longrightarrow SO_4^{2-} (\text{or } SO_4^{2-} + {}^{\cdot}OH + H^+) \quad (13)$$

But the approach of CH_3COO^- ion demonstrated the adverse effect. Due to addition of CH_3COONa salt in the solution, the medium becomes basic and degradation decreases which is discussed in earlier. It also inhibits the formation of ${}^{\cdot}OH$ by the photo-kolbe reaction [49, 50] via the Eqs. (14)-(16).

4.6 Effect of Scavengers

In order to explore the different species involved and the main agent responsible for the photocatalytic degradation of RhB, the reaction is followed in presence and absence of scavenger of h^+, ${}^{\cdot}O_2^-$ and ${}^{\cdot}OH$ radicals. In the trapping experiments each scavenger was added at equal concentration in separate experimental solutions containing same composition of dye, H_3O^+ and catalyst to observe the direct influence of the scavengers on the degradation rates. As shown in the Fig. 10, the degradation efficiency of RhB is found to decrease rapidly from 98.66% to 19.85% with addition of Na_2EDTA which is a scavenger (trapper) of hole. The rate of arresting the reaction decreases in the order EDTA > BQ > IPA > No scavenger, indicating that the hole is the main species for degradation, followed by $O_2^{\cdot-}$ and ${}^{\cdot}OH$. The apparent rate constant (k) without addition of scavenger is 0.07414 min^{-1} and for EDTA k values decreases to 0.00072 min^{-1}. A little decrease of rate constant for BQ (0.0565) and IPA (0.0682) is observed indicating h^+ is

the main reactive species and $\cdot O_2^-$ $\cdot OH$ radicals plays minor role for the rapid degradation of RhB.

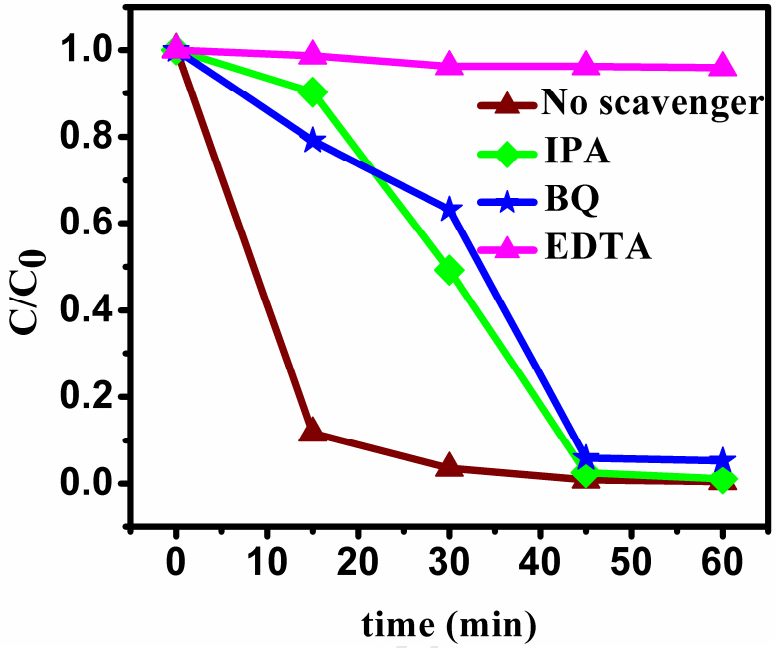

Fig. 10 Effect of different radical scavengers on the degradation of RhB over α-β Bi_2O_3 under sunlight.

4.7 Identification of products of degradation of RhB with α-β Bi_2O_3 photocatalyst

The RhB and intermediates generated in the photo-oxidative process were analyzed with a JASCO liquid chromatograph (HPLC) equipped a multi-wavelength detector and crestpak C18S column in the mixed eluent CH_3OH: H_2O = 1:1 by volume. The detected intermediates by HPLC are shown in the Figure 11a and b.

Fig. (a)

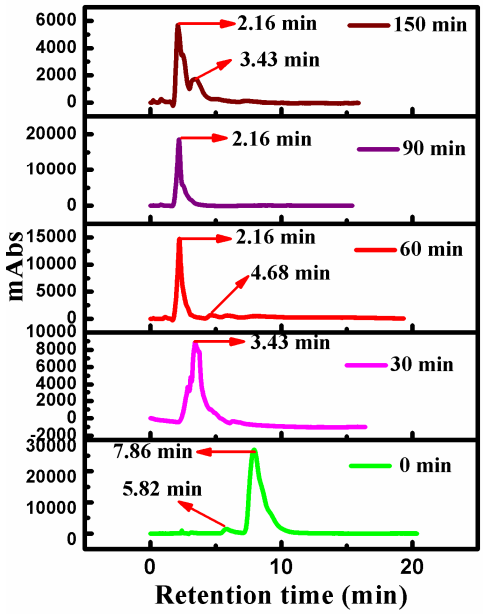

(b)

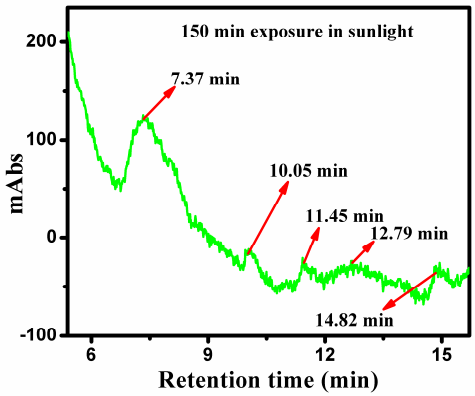

Fig. 11. (a) Identification of the solute components in the solution undergoing photo catalytic degradation of RhB for different time extents by HPLC (under sunlight irradiation) (b) Some parts of profiles of figure 10 (a) (for the solution undergoes 150 min exposure of sunlight) with greater resolution to show the dominant products.

Five main components which have retention times (/min) 7.86 (m/z = 443, RhB), 5.82 (m/z = 387, DR), 4.68 (m/z = 387, EER), 3.43 (m/z = 359, ER) and 2.16 (m/z = 301) have been identified from the solution subjected to 90 min irradiation of sunlight. The absorbance (mAbs) of the peak obtained at retention time (/min)7.86 and 5.82 decrease and gradually lose m/z values of 28 and 45 which are the values of an ethyl group and one COOH group to form degraded products as presented in scheme 3. On expose of RhB solution to sunlight for 150

minute, destruction of xanthate ring occurs with formation of mainly adipic acid (Rt = 11.54 min, m/z = 146), phthalic acid (Rt = 12.89 min, m/z = 166), 2- hydroxyl penta-di-ioic acid (Rt = 10.56 min, m/z = 148) and 2, 5 di hydroxyl benzoic acid (R_t = 14.83 min, m/z = 154). All these products found from HPLC are well matched with the results of the other researcher [33, 51]. To obtain more information about the highly polar intermediates having small molar mass that could not be identified properly by HPLC, the products are further analyzed by HRMS technique. Some degradation products from HRMS, having strong sign at m/z 391, 387, 370, 301, 290, 197, 151, 149, 164 are presented in Fig. 12 and scheme 3. According to the relevant literature reported and combining with MS analysis, the peaks at m/z 443.4, 415.3, 387.3and 359.3 were identified as RhB and its N-deethylated intermediates namely, N,N,N'-triethyl rhodamine (DER), N, N-diethylrhodamine (DR), N-ethyl-N-ethylrhodamine (EER) and N-ethyl rhodamine (ER) respectively. Among them, DR and EER are pair of isomers [52] and the compounds having m/z = 370, 301 and 290 are the products of deethylation followed by de carboxylation. In our present study, HRMS provides the solid evidence for the formation N- dethylated products and cleavage of chromophore structure of RhB. Fig. 8a and b illustrates that absorption maxima of RhB dye shifted from 554 nm to 496 nm (hypsochromic shift). This shift of absorption band was presumed to result from the formation of a series of N-deethylated intermediates in a step wise manner [53, 54]. The color of the suspension changed gradually from pink to light green during the progress of the reaction and finally becomes colorless. This indicates that the α-β Bi_2O_3 photocatalyst enhances significantly the de- ethylation process in comparison to the cleavage of ring structures [55].

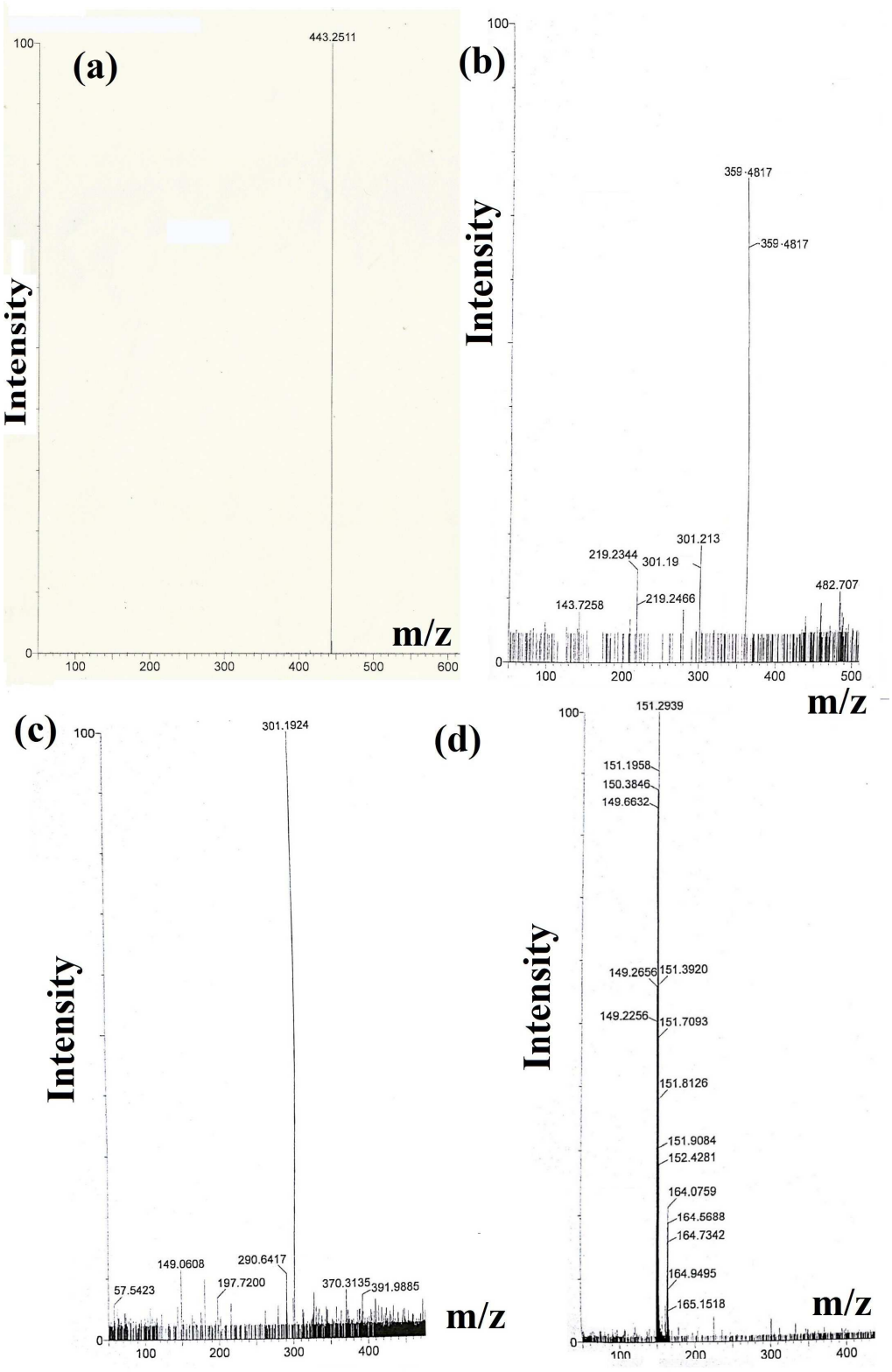
(a)
443.2511
Intensity
m/z
100
0
100
200
300
400
500
600
(b)
359.4817
359.4817
301.213
219.2344
301.19
219.2466
143.7258
482.707
Intensity
m/z
100
0
100
200
300
400
500
(c)
301.1924
149.0608
290.6417
197.7200
57.5423
370.3135
391.9885
Intensity
m/z
100
0
100
200
300
400
(d)
151.2939
151.1958
150.3846
149.6632
149.2656
151.3920
149.2256
151.7093
151.8126
151.9084
152.4281
164.0759
164.5688
164.7342
164.9495
165.1518
Intensity
m/z
100
0
100
200
300
400

Fig. 12. HRMS spectra of RhB solution under irradiation for (a) 0 min (b) 30 min (c) 60 min (d) 210 min.

Scheme 2.

Photo catalytic degradation pathway of RhB by α-β Bi_2O_3 photocatalyst.

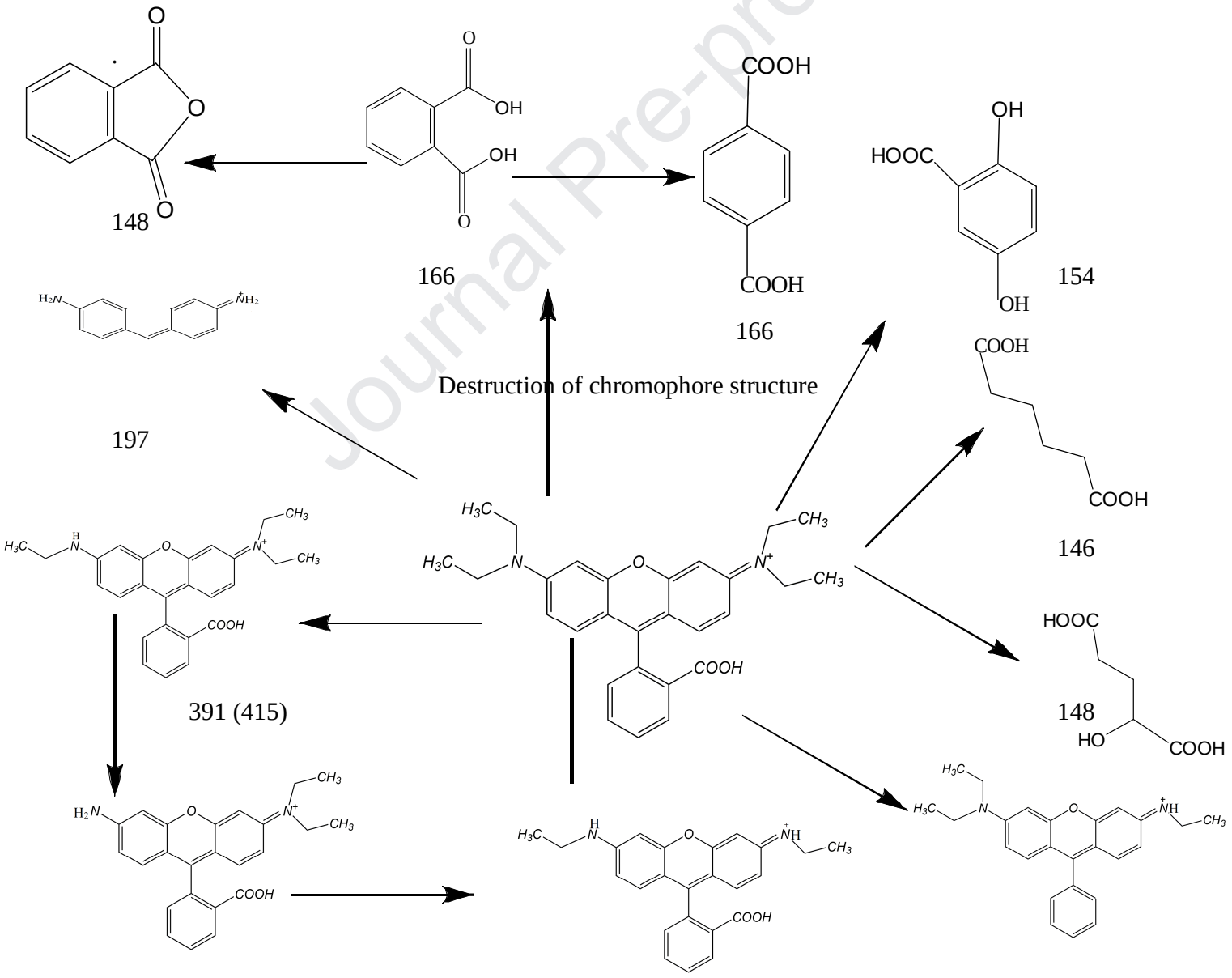

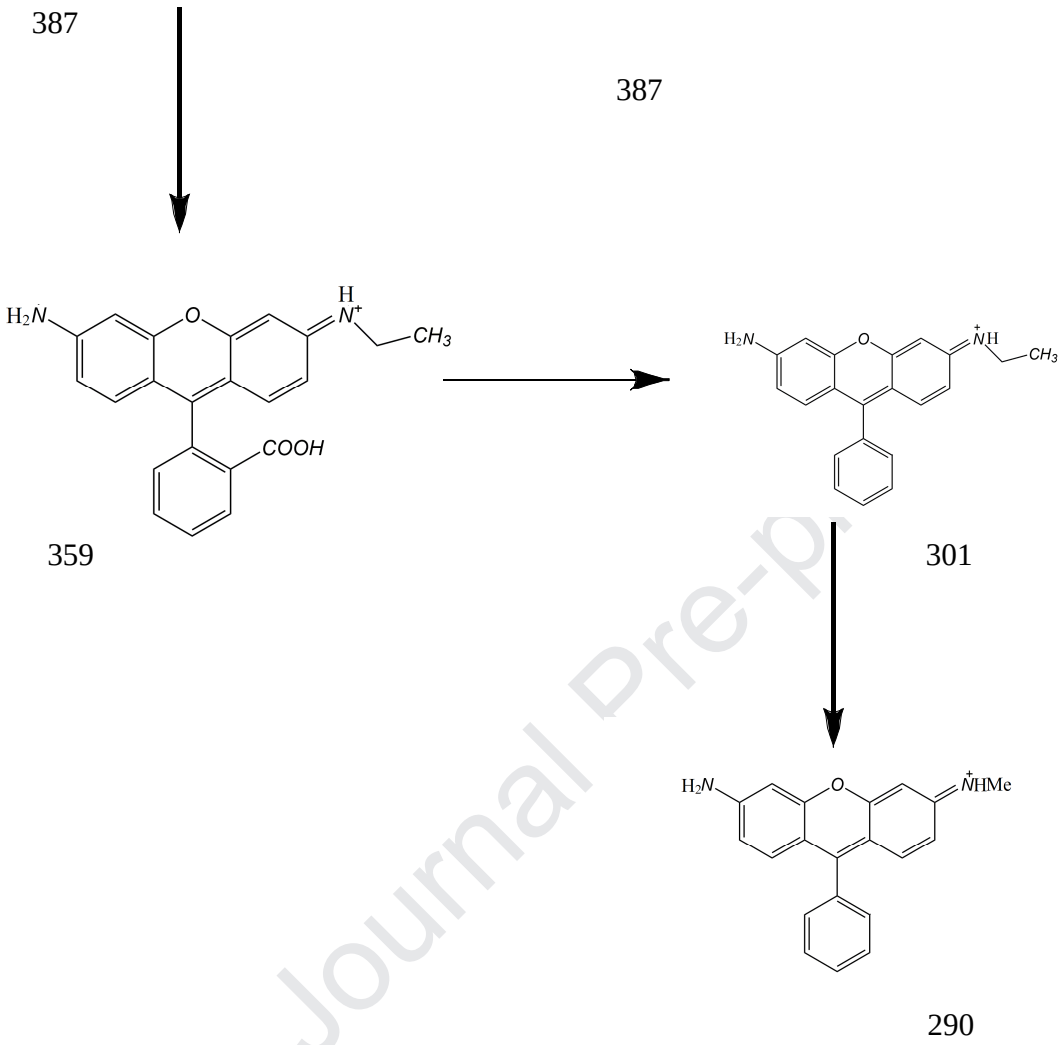

Deethylation products

4.8. Mechanism of photo degradation

There are two possible photo chemical mechanisms: (a) photocatalytic process (b) photo sensitization process. In photo catalytic process, RhB can be degraded by direct interaction with strong oxidizing hole originating from the hybridization of the Bi 6s and 2p orbital. Our previous report [12] illustrates how the hole created by α-β Bi_2O_3 photocatalyst becomes the main source

of ·OH and function as the main degrading species of RhB dye. Here ·OH and $O_2^{\bullet-}$ radical help in the cleavage of conjugated structures (path b). On the other hand, RhB dye itself can absorb sunlight and goes to the excited state of dye (RhB*). This excited dye can transfer electron to the CB of α-Bi_2O_3 to form $RhB^{+\cdot}$ as the LUMO of RhB and CB of α-Bi_2O_3 are -1.42 V and 0.33 V vs NHE [56, 57]. The $RhB^{+\cdot}$ reacts with adsorbed dye to form deethylated products (path a) by the photo sensitization process (shown in Fig. 13). Again, the adsorbed molecular oxygen on the catalyst captures electron from the CB of Bi_2O_3 to form $O_2^{\bullet-}$. The oxidant $O_2^{\bullet-}$ radical reacts with adsorbed dye to degrade it. The holes in the HOMO react with adsorbed H_2O to form •OH radical. It is worth mentioning that the photosensitization degradation of RhB occurs commonly via process involving N-deethylated step compared to photocatalytic process [58]. Therefore, de ethylated products are found in this study indicating that photosensitization process plays a vital role in the overall degradation of RhB although both path a and b might be operating simultaneously. In presence of Cl^- in the system, α-Bi_2O_3 is gradually converted to BiOCl in aqueous medium as observed in our previous study [12]. Although α or β Bi_2O_3 comprise type 1 semiconductor junction, in situ generation of BiOCl makes the α or β Bi_2O_3 / BiOCl as type II junction and thus electrons are accumulated at the conduction band of β Bi_2O_3, holes are accumulated at the valence band of BiOCl, making effective separation of primary charge carriers. A plausible scheme stating the two paths are shown below.

Path a

$$RhB + hv \longrightarrow RhB^*$$

$$RhB^* + Bi_2O_3 \longrightarrow Bi_2O_3(e) + RhB^{\cdot +}$$

$$RhB^{\cdot +} + \text{Adsorbed dye} \longrightarrow \text{N-deethylated products}$$

Path b

$$Bi_2O_3(\alpha/\beta) \xrightarrow{Cl^-} BiOCl$$

$$\beta\ Bi_2O_3 + hv \xrightarrow{H_2O} \beta\ Bi_2O_3\ (e) + \beta\ Bi_2O_3\ (h^+)$$

$$BiOCl + \beta\ Bi_2O_3\ (h^+) \longrightarrow BiOCl\ (h^+) + \beta\ Bi_2O_3$$

$$BiOCl\ (h^+) + \text{RhB/ N-deethyalated products} \longrightarrow \text{Clevage of structures}$$

$$\beta\ Bi_2O_3\ (e) + O_2 \longrightarrow \beta\ Bi_2O_3 + O_2^{\cdot -}$$

$$h^+ + H_2O \longrightarrow {}^{\cdot}OH + H^+$$

$$O_2^{\cdot -}/{}^{\cdot}OH + RhB \longrightarrow \text{RhB oxidation products}$$

In our system both nitrogen centre radical path ‘a’ and carbon centered radical path ‘b’ through initial formation of $O_2^{\bullet -}$ and •OH, occur simultaneously. But it seems that the reactions through path ‘a’ occur more effectively at the initial stage of first 90 minutes for which the N-deethylated products are the main intermediates. After 90 minute, destruction of chromophoric structure through path ‘b’ dominates over path a and finally after 150 minutes we get small compounds containing a phenyl backbone like phthalic acid (166), phthalic anhydride (148), dihydroxy benzoic acid (154) etc. Since de ethylated products are mainly formed after exposure of radiation for small time interval (60 min, 90 min) as obtained from mass and HPLC studies, it may be inferred that the breaking of ring structure is easy after de-ethylation.

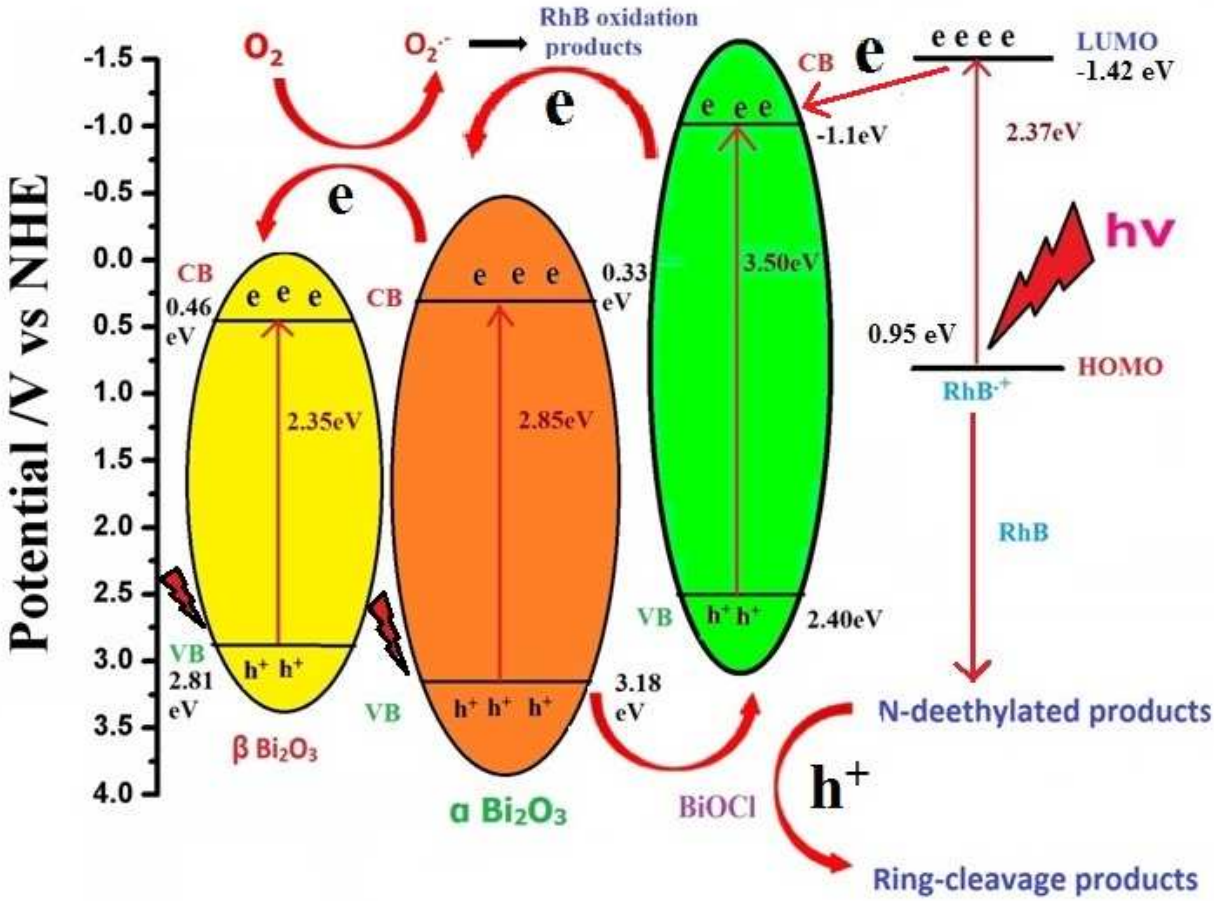

Fig. 13. Plausible charge-transfer mechanism and photo catalytic degradation of RhB.

5. Conclusion

We have successfully synthesized biphasic heterojunctions having various molar ratios of α and β forms of Bi_2O_3 by changing the concentration of bismuth nitrate precursor in glycerol solution following facile solvothermal method without calcination. The X-ray diffraction and microscopic studies reveal that the dimension of nanosphere and nanorod of two different forms produced are gradually increased with the initial concentration of the precursor. The optimum dosage of the synthesized catalyst, pH and H_2O_2 concentration for better photocatalytic degradation of 10 ppm RhB are found to be 0.5 gL^{-1}, 4 and 2 mM respectively. The efficiency of the degradation by the best α-β Bi_2O_3 composite is increased from 89% at pH 5 to 98% at pH 4 in 180 min under sunlight illumination. Addition of NO_3^- and Cl^- salts increase the photocatalytic degradation of RhB by 12.1% and 9.0 %, while SO_4^{2-} and CH_3COO^- salts decrease degradation in comparison to that found without salt addition. These results infer strong adsorption of NO_3^- and Cl^- ions on the α-β Bi_2O_3 surface which seemingly facilates the greater generation of $^{\cdot}OH$ radicals. The greater presence of N-deethylated products (DER, EER, DR, R) as confirmed from HRMS and HPLC techniques, indicates that the degradation mainly proceeds via photosensitization induced photocatalytic mechanism. In this process, RhB dye produce $RhB^{\cdot+}$ and $^{\cdot}OH$ radical which might be the main degrading agent. The decarboxylation and the ring cleavage of RhB were also observed on irradiation of sunlight for 150 min under optimized condition. The main nontoxic products are adipic acid, phthalic acid, 2- hydroxyl penta-di-ioic acid and 2, 5 di hydroxyl benzoic acid which are again mineralized to CO_2 and H_2O on more exposure to sunlight.

Acknowledgments

This work was supported by Jadavpur University (JU), India and University Grant Commission (UGC, Grant no. 2121510262) Delhi, India. Thanks to Prof. S. Das of JU for helping Chromatography Studies.

Reference

[1] E. Kevin, O. Dionysios, D. Dionysiou, Advanced oxidation processes for water treatment, J. Phys. Chem. Lett. 3 (2012) 2112−2113.

[2] S.H.S. Chan, T.Y. Wu, J.C. Juan, C.Y. Teh, Recent developments of metal oxide semiconductors as photocatalysts in advanced oxidation processes (AOPs) for treatment of dye waste-water, J. Chem. Technol. Biotechnol. 86 (2011) 1130–1158.

[3] J. Schneider, M. Matsuoka, M. Takeuchi, J. Zhang, Y. Horiuchi, M. Anpo, D.W. Bahnemann, Understanding TiO_2 photocatalysis: mechanisms and materials, Chem. Rev. 114 (2014) 9919−9986.

[4] A. Mclaren, T. Valdes-solis, G.Q. Li, S.C. Tsang, Shape and size effects of ZnO nanocrystals on photocatalytic activity, J. Am. Chem. Soc. 131 (2009) 12540–1541.

[5] M. Muruganandham, R. Amutha, G.J. Lee, S.H. Hsieh, J.J. Wu, M. Sillanpää, Facile fabrication of tunable Bi_2O_3 self-assembly and its visible light photocatalytic activity, J. Phys. Chem. C 116 (2012) 12906–12915.

[6] F. Motahari, M.R. Mozdianfard, F. Soofivand, M. Salavati-Niasari, NiO nanostructures: synthesis, sharacterization and photocatalyst application in dye wastewater treatment, RSC Adv. 4 (2014) 27654–27660.

[7] K. Nakata, A. Fujishima, TiO_2 photocatalysis: design and applications, J. Photochem. Photobiol. C Photochem. Rev. 13 (2012) 169–189.

[8] L. Leontie, M. Caraman, M. Alexe, C. Harnagea, Structural and optical characteristics of bismuth oxide thin films, Surf. Sci. 507 (2002) 480–485.

[9] M. Drache, P. Roussel, J.P. Wignacourt, Structures and oxide mobility in Bi−Ln−O materials: heritage of Bi_2O_3, Chem. Rev. 107 (2007) 80–96.

[10] Y. Shi, L. Luo, Y. Zhang, Y. Chen, S. Wang, L. Li, Y. Long, F. Jiang, Synthesis and characterization of α/β-$Bi_2O_3$with enhanced photocatalytic activity for 17α-Ethynylestradiol, Ceram. Int. 43 (2017) 7627–7635.

[11] T.A. Gadhi, A. Hernández-Gordillo, M. Bizarro, P. Jagdale, A. Tagliaferro, S.E. Rodil, Efficient α/β-Bi_2O_3 composite for the sequential photodegradation of two-dyes mixture, Ceram. Int. 42 (2016) 13065–13073.

[12] K.K. Bera, R. Majumdar, M. Chakraborty, S.K. Bhattacharya, Phase control synthesis of α, β and α/β Bi_2O_3 hetero- junction with enhanced and synergistic photocatalytic activity on degradation of a toxic dye, Rhodamine-B under natural sunlight, J. Hazard. Mater. 352 (2018) 182-191.

[13] R. Chen, Z.R. Shen, H. Wang, H.J. Zhou, Y.P. Liu, D.T. Ding, T.H. Chen, Fabrication of mesh-like bismuth oxide single crystalline nanoflakes and their visible light photocatalytic activity, J. Alloys Compd. 509 (2011) 2588–2596.

[14] X. Xiao, R. Hu, C. Liu, C. Xing, C. Qian, X. Zuo, J. Nan, L. Wang, Facile large-scale synthesis of β-Bi_2O_3 nanospheres as a highly efficient photocatalyst for the degradation of acetaminophen under visible light irradiation, Appl. Catal. B Environ. 141 (2013) 433–443.

[15] Y. Qiu, M. Yang, H. Fan, Y. Zuo, Y. Shao, Y. Xu, X. Yang, S. Yang, Phase-transitions of α- and β-Bi_2O_3nanowires, Mater. Lett. 65 (2011) 780–782.

[16] J. Hou, C. Yang, Z. Wang, W. Zhou, S. Jiao, H. Zhu, In situ synthesis of α–β phase heterojunction on Bi_2O_3 nanowires with exceptional visible-light photocatalytic performance, Appl. Catal. B Environ. 142 (2013) 504–511.

[17] K. Brezesinski, R.Ostermann, P. Hartmansin, J. Brezesinski, Exceptional photocatalytic activity of ordered mesoporous β-Bi_2O_3 thin films and electrospun nanofiber, Chem. Mater. 22 (2010) 3079–3085.

[18] S. Roy Chowdhury, S. Ghosh, S.K. Bhattachrya, Enhanced and synergistic catalysis of one-pot synthesized palladium-nickel alloy nanoparticles for anodic oxidation of methanol in alkali, Electrochim. Acta 250 (2017) 124 –134.

[19] W. Ma, N. Wang, Y. Lu, Z. Lu, X. Tang, S. Li, Synthesis of magnetic biomass carbon-based Bi_2O_3 photocatalyst and mechanism insight by a facile microwave and deposition method. New J. Chem. 43 (2019) 2888-2898.

[20] R. Ji, C. Ma, W. Ma Y. Liu, Z. Zhu, Y. Yan, Z-scheme MoS_2/Bi_2O_3 heterojunctions: enhanced photocatalytic degradation performance and mechanistic insight. New J. Chem. 43(2019) 11876-11886.

[21].F. He, J. wang, D. Deng, Effect of Bi_2O_3 on structure and wetting studies of Bi_2O_3–ZnO–B_2O_3 glasses, J. Alloy. Compd. 509 (2011) 6332–6336.

[22] S. Wang, Y. Guan, L. Wang, W. Zhao, H. He, J. Xiao, S. Yang, C. Sun, Fabrication of a novel bifunctional material of BiOI/Ag_3VO_4 with high adsorption–photocatalysis for efficient treatment of dye wastewater, Appl. Catal. B 168 (2015) 448–457.

[23] M. Popa, A. Totovana, L. Popescu, N. Dragan, M. Zaharescu, Reactivity of the Bi, Sr, Ca, Cu oxalate powders used in BSCCO preparation, J. Eur. Ceram. Soc. 18 (1998) 1265–1271.

[24] Y. Sun, W. Wang, L. Zhang, Z. Zhang, Design and controllable synthesis of α-/γ-Bi_2O_3 homojunction with synergetic effect on photocatalytic activity. Chem. Eng. J. 211 (2012) 161-167.

[25] A.H ezam, , K., Namratha, Q. A., Drmosh, Z. H., Yamani, K.Byrappa, Synthesis of heterostructured Bi_2O_3–CeO_2–ZnO photocatalyst with enhanced sunlight photocatalytic activity. Ceram. Int. 43(2017) 5292-5301.

[26] C. Wang, C. Shao, L. Wang, L. Zhang, X. Li, Y. Liu, Electrospinning preparation, characterization and photocatalytic properties of Bi_2O_3 nanofibers, J. Colloid Interf. Sci. 333 (2009) 242–248.

[27] Y. Xiong, M. Wu, J. Ye, Q. Chen, Synthesis and luminescence properties of hand-like α-Bi_2O_3 microcrystals, Mater. Lett. 62 (2008) 1165–1168.

[28] H. Feng, H. Zijun, X. Junlin, L. Yuhui, IR and Raman spectra properties of Bi_2O_3-ZnO-B_2O_3-BaO quaternary glass system, Am. J. Anal. Chem. 5 (2014) 1142–1150.

[29] Q. Huang, S. Zhang, C. Cai, B. Zhou, β- and α-Bi_2O_3 nanoparticles Synthesized via microwave-assisted method and their thotocatalytic activity towards the degradation of Rhodamine B, Mater. Lett. 65 (2011) 988–990.

[30] Y. Lu, Y. Zhao, J. Zhao, Y. Song, Z. Huang, F. Gao, Y. Li, Induced aqueous synthesis of metastable β-Bi_2O_3microcrystals for visible-light photocatalyst study, Cryst. Growth Des. 15 (2015) 1031–1042.

[31] L. Shan, G. Wang, D. Li, X. San, L. Liu, L. Dong, Z. Wu, Band alignment and enhanced photocatalytic activation of α/β-Bi_2O_3 heterojunctions via in situ phase transformation, Dalton Trans. 44 (2015) 7835-7843.

[32] R. Irmawati, M.N.N. Nasriah, Y.H. TaufigYap, S.B. A. Hamid, Characterization of bismuth oxide catalysts prepared from bismuth trinitrate pentahydrate: influence of bismuth concentration, Catal. Today 93 (2004) 701–709.

[33] H.E. Zhong, Y. Shaogui, J.U. Yongming, S. Cheng, Microwave photocatalytic degradation of Rhodamine B using TiO_2 supported on activated carbon: Mechanism implication. J. Environ. Sci. 21(2009) 268–272.

[34] F. Chen, J. Zhao, H. Hidaka, Highly selective deethylation of Rhodamine B: adsorption and photooxidation pathways of the dye on the TiO_2/SiO_2 composite photocatalyst. Int. J. Photoenergy 5 (2003) 209–217.

[35] T. Selvamani, S. Anandan, L. Granone, D. W. Bahnemann, M. Ashokkumar, Phase-controlled synthesis of bismuth oxide polymorphs for photocatalytic applications. *Mat. Chem. Front. 2* (2018) 1664-1673.

[36] C. Lops, A. Ancona, D. Cesare, K. Dumontel, B. Garino, N. Canavese, V. Cauda, Sonophotocatalytic degradation mechanisms of Rhodamine B dye via radicals generation by micro-and nano-particles of ZnO. Appl. Catal. B Environ. 243 (2019) 629-640.

[37]. S. Sood, A. Umar, S.K. Mehtaa, S.K. Kansal, α-Bi_2O_3 nanorods: an efficient sunlight active photocatalyst for degradation of Rhodamine B and 2,4,6-trichlorophenol. Ceram. Int. 41 (2015) 3355–3364.

[38] T. Kou, C. Jin, C. Zhang, J. Sun, Z. Zhang, Nanoporous Core-Shell Cu@Cu_2O Nanocomposites with Superior Photocatalytic Properties towards the Degradation of Methyl Orange. RSC Adv. 33 (2012) 12636–12643.

[39] P. Mohammadyari, A. Nezamzadeh-Ejhieh, Supporting of mixed ZnS-NiS semiconductors

onto clinoptilolite nano-particles to improve its activity in photodegradation of 2-nitrotoluene, RSC Adv. 5 (2015) 75300–75310.

[40] H.R Pouretedal, A. Norozi, M.H. Keshavarz, A. Semnani, Nanoparticles of zinc sulfide doped with manganese, nickel and copper as nanophotocatalyst in the degradation of organic dyes. J. Hazard. Mater. 162 (2009) 674–681.

[41] F. H. AlHamedi, M. A Rauf, S. S. Ashraf, Degradation studies of Rhodamine B in the presence of UV/H_2O_2. Desalination 239 (2009) 159–166.

[42] B. Katherine, A. Benedict, S. McFall, C. Anastasio, Quantum Yield of Nitrite from the Photolysis of Aqueous Nitrate above 300 nm, Environ. Sci. Technol., 51 (2017) 4387−4395.

[43] W. Hua, F. Wub, W. Liua, J. Liuc, Nitrate-induced Photodegradation of Colorants and the Corresponding Mechanisms Study, J. Adv. Oxid. Technol. 21 (2018) 285-296.

[44] T.T. Nga Phan, A.N. Nikoloski, P.A. Bahri, D. Li, Adsorption and photo-Fenton catalytic degradation of organic dyes over crystalline $LaFeO_3$-doped porous silica. RSC Adv. 8 (2018) 36181-36190.

[45] S. Azimia, A. Nezamzadeh-Ejhieh, Enhanced activity of clinoptilolite-supported hybridized PbS–CdS semiconductors for the photocatalytic degradation of a mixture of tetracycline and cephalexin aqueous solution, J. Mol. Catal. A: Chemical 408 (2015) 152–160

[46] P.V. Nidheesh, R. Gandhimathi, N.S. Sanjini, $NaHCO_3$ enhanced Rhodamine B removal from aqueous solution by graphite–graphite electro Fenton system, Sep. Purif. Technol. 132 (2014) 568–576

[47] A. Dhanya, K. Aparna, Synthesis and evaluation of TiO_2/Chitosan based hydrogel for the adsorptional photocatalytic degradation of Azo and anthraquinone dye under UV light irradiation

Procedia Technol. 24 (2016) 611 – 618

[48] Factors influencing the photocatalytic degradation of Rhodamine B by TiO_2-coated non-woven paper, N. Barka, S. Qourzal, A. Assabbane, A. Nounah, Y. Ait-Ichou . J. Photochem. Photobiol. 195 (2008) 346–351

[49] B. Kraeutler, C.D. Jaeger. A.J. Bard, Direct observation of radical intermediates in the photo-Kolbe reaction-heterogeneous photocatalytic radical formation by electron spin resonance. J. Am. Chem. Soc. 100 (1978) 4903-4905.

[50] S. Sato,Photo-Kolbe Reaction at Gas-Solid Interfaces. J. Phys. Chem., 87 (1983) 3531-3537.

[51] F. Chen, J. Zhao, H. Hidaka, Highly selective deethylation of Rhodamine B: adsorption and photooxidation pathways of the dye on the TiO_2/SiO_2 composite photocatalyst, *I*nt. J. Photoenergy 5 (2003) 209–217.

[52] Y. Zhang, J. Zhou, Biomaterials photodegradation pathway of Rhodamine B with novel Au nanorods @ ZnO microspheres driven by visible light irradiation, J. Mater. Sci. 53 (2018) 3149–3162.

[53] T. Watanabe, T. Takizawa, K. Honda, Photocatalysis through excitation of adsorbates. 1. Highly efficient Ndeethylation of rhodamine B adsorbed to cadmium sulfide, J. Phys. Chem. 81 (1977)1845–1851.

[54] T. Takizawa, T. Watanabe, K. Honda, Photocatalysis through excitation of adsorbates: A comparative study of Rhodamine B and methylene blue on cadmium sulfide, J. Phys. Chem. 82 (1978) 1391–1396.

[55] H. Fu, S. Zhang, Photocatalytic Degradation of RhB by Fluorinated Bi_2WO_6 and Distributions of the Intermediate Products, Environ. Sci. Technol. 42 (2008) 2085–2091.

[56] L. Pan, J. Zou, X. Liu, X. Liu, S. Wang, X. Zhang, L. Wang, Visible-light-induced photodegradation of Rhodamine B over hierarchical TiO_2: effects of storage period and water-mediated adsorption switch, Ind. Eng. Chem. Res. 51 (2012) 12782-12786.

[57] Y. Xu, M. Schoonen, The absolute energy positions of conduction and valence bands of selected semiconducting minerals, Am. Mineral. 85 (2000) 543-556

[58] P. Lei, C. Chen, J. Yang, W. Ma, J. Zhao, L. Zang, Degradation of dye pollutants by immobilized polyoxometalate with H_2O_2 under visible-light irradiation. Environ. Sci. Technol. 39 (2005) 8466–8474.

Declaration of interests

☐ The authors declare that they have no known competing financial interests or personal relationships that could have appeared to influence the work reported in this paper.

☐The authors declare the following financial interests/personal relationships which may be considered as potential competing interests:

The authors declare that they have no known competing financial interests or personal relationships that could have appeared to influence the work reported in this paper.